

Local Projections Inference with High-dimensional Covariates without Sparsity

Jooyoung Cha^{*†}

October 4, 2024

Abstract

This paper presents a comprehensive local projections (LP) framework for estimating future responses to current shocks, robust to high-dimensional controls without relying on sparsity assumptions. The approach is applicable to various settings, including impulse response analysis and difference-in-differences (DiD) estimation. While methods like LASSO exist, they often rely on sparsity assumptions—most parameters are exactly zero, limiting their effectiveness in dense data generation processes. I propose a novel technique incorporating high-dimensional covariates in local projections using the Orthogonal Greedy Algorithm with a high-dimensional AIC (OGA+HDAIC) model selection method. This approach offers robustness in both sparse and dense scenarios, improved interpretability, and more reliable causal inference in local projections. Simulation studies show superior performance in dense and persistent scenarios compared to conventional LP and LASSO-based approaches. In the empirical application, applying the proposed method to [Acemoglu, Naidu, Restrepo, and Robinson \(2019\)](#), I show efficiency gains and robustness to a large set of controls. Additionally, I examine the effect of subjective beliefs on economic aggregates, demonstrating robustness to various model specifications. A novel state-dependent analysis reveals that inflation behaves more in line with rational expectations in good states, but exhibits more subjective, pessimistic dynamics in bad states.

*Jooyoung Cha: jooyoung.cha@vanderbilt.edu. Department of Economics, Vanderbilt University

†I am grateful to Yuya Sasaki, Atsushi Inoue, Harold D. Chiang, Ke-Li Xu, and Vadim Marmer for their advice and guidance. I also thank Chuanping Sun and participants of the New York Camp Econometrics XVIII, SETA 2024 meeting, IAAE 2024 China, IAAE 2024 Greece, and Econometric Study Group Bristol for their helpful comments and suggestions.

1 Introduction

Impulse responses analyze how a shock, such as a change in interest rates, affects various aspects of the economy over time. Knowing how different parts of the economy respond to shocks, such as policy changes or natural shocks, helps policymakers make informed decisions and businesses prepare for potential impacts. In recent years, local projections (LPs), introduced by [Jordà \(2005\)](#), have gained considerable attention as a flexible alternative to traditional Vector Autoregression (VAR) models. LPs directly estimate the relationship between shocks and future outcomes, offering simplicity and intuitive interpretability.

As the use of LPs has grown, so has the recognition of the need for high-dimensional controls in these models. While methods like LASSO have been proposed to handle high-dimensional covariates, they heavily rely on sparsity assumptions—the idea that most parameters are exactly zero. Recent work by [Adamek, Smeekes, and Wilms \(2023, 2024\)](#) proposed using a debiased or desparsified LASSO in time series and local projections with weaker form of sparsity, but their approach still faces challenges in scenarios with dense data generating processes (DGPs). Recent studies by [Giannone, Lenza, and Primiceri \(2021\)](#) and [Kolesár, Müller, and Roelsgaard \(2023\)](#) have raised significant concerns about the validity and reliability of these assumptions in economic models, challenging their applicability in many empirical settings.

This paper presents a novel approach to local projections that incorporates high-dimensional covariates without relying on sparsity constraints. The proposed method adapts the Orthogonal Greedy Algorithm with a High-Dimensional Akaike Information Criterion (OGA+HDAIC), originally developed by [Ing \(2020\)](#), to the context of local projections. In contrast to LASSO-based methods, the proposed approach allows parameters to be nonzero but assumes they decay toward zero as dimensionality grows. This assumption is more flexible and is automatically satisfied by autoregressive processes, making it especially suitable for time series settings. This approach offers a more versatile framework that can handle both sparse and dense scenarios, which is ideal for economic time series analysis.

The Orthogonal Greedy Algorithm proposed in this paper offers several advantages over existing methods, particularly in terms of interpretability. Unlike Principal Component methods ([Stock and Watson, 2002](#)), the proposed method prioritizes variables based on their cross-sectional explanatory power. This feature not only enhances the model's interpretability but also provides valuable insights into the most influential covariates in impulse response dynamics. Such information is crucial for economists and policy-

makers seeking to understand shock propagation mechanisms in the economy. Recent work by [Dinh, Nibbering, and Wong \(2024\)](#) has applied random subspace methods in this domain, sharing the motivation to address high-dimensional controls in local projections. While their approach offers empirical insights, the proposed method provides a statistical inference theory in addition to practical applicability.

From a theoretical perspective, this paper contributes to the literature by extending the OGA+HDAIC method of [Ing \(2020\)](#) to the context of local projections. My coauthors and I previously adapted this method to a cross-sectional double machine learning framework ([Cha, Chiang, and Sasaki, 2023](#)). In the current paper, I further develop this approach for the time series context by incorporating explicit assumptions on the dependence structure, using the near epoch dependence (NED) assumption as employed by [Adamek et al. \(2023, 2024\)](#). A key advantage of using the NED assumption is that it inherits the mixingale properties that I employ in deriving the error bounds.¹ I leverage the triplex inequality from [Jiang \(2009\)](#) in conjunction with the results in [Ing \(2020\)](#) to derive the inference of the proposed method. In deriving the inference, I incorporate a double selection method ([Belloni, Chernozhukov, and Hansen, 2013](#)), which effectively addresses potential overfitting issues in high-dimensional dynamics involving lagged covariates and outcomes. This framework enables the derivation of error bounds and asymptotic Gaussianity, providing both theoretical guarantees and practical implementation strategies.

Building on the solid statistical background, the proposed method's ability to handle high-dimensional controls has important implications for identification, addressing several key challenges. From a causal identification perspective, [Angrist, Jordà, and Kuersteiner \(2018\)](#) proposed interpreting local projections as causal parameters, with the key identifying assumption being unconfoundedness. The inclusion of large sets of covariates, which the proposed method efficiently manages, enhances the plausibility of this assumption ([D'Amour, Ding, Feller, Lei, and Sekhon, 2021](#); [Rosenbaum and Rosenbaum, 2002](#)). By incorporating a comprehensive set of potential confounders, we can more confidently assume unconfoundedness, strengthening the causal interpretation of the estimates.

In terms of identifying structural impulse responses, the proposed method addresses the invertibility condition by essentially solving an omitted variable bias problem ([Stock and Watson, 2016](#), p. 450). When relying on the LP-VAR equivalence results from [Plagborg-Møller and Wolf \(2021\)](#), we must consider the bias term arising from finite lag approxima-

¹I have benefited enormously from the comprehensive foundation of dependence concepts and properties in the exquisite textbook [Davidson \(1994\)](#).

tions. This bias decreases as the number of included lags increases, further justifying the use of high-dimensional controls.

In a Difference-in-Differences (DiD) framework, [Dube, Girardi, Jorda, and Taylor \(2023\)](#) extend local projections to estimate DiD parameters, with the parallel trends assumption the key assumption for identification. Building on this identification scheme, my framework introduces high-dimensional controls, which greatly enhance the credibility of the conditional parallel trends assumption. As highlighted by [Heckman, Ichimura, and Todd \(1997\)](#); [Heckman, Ichimura, Smith, and Todd \(1998\)](#), factors like demographic differences or regional economic conditions can lead to non-parallel trends, introducing bias into traditional DiD estimates. By incorporating a rich set of covariates, high-dimensional methods address these potential biases, making the conditional parallel trends assumption more plausible.

By addressing these identification challenges through the inclusion of high-dimensional controls, the proposed method enhances their interpretability and potential for causal inference. In the following Section 2, I will demonstrate how these high-dimensional methods are applied to various identification schemes, including structural impulse response estimation and DiD approaches, providing a comprehensive framework for modern empirical analysis.

To demonstrate the effectiveness of this approach, I conduct illustrative simulation studies comparing the proposed method with conventional LP and LASSO-based approaches. For the simulation design, I adapt from [Montiel Olea and Plagborg-Møller \(2021\)](#), where they proposed lag augmentation—adding one more lag as controls than the true autoregressive model suggests, to achieve robust inference with persistent data a longer horizons. I adopt lag augmentation for all the methods to see if such robust inference holds in finite samples. Simulation results suggest that the proposed method performs consistently well, especially in dense and more persistent scenarios. This is particularly relevant for macroeconomic applications where data often exhibit high persistence and complex interdependencies.

In empirical applications, I apply the proposed method to the following two studies. First, I revisit the analysis of [Acemoglu et al. \(2019\)](#) on the causal effects of democracy on economic growth. The proposed method demonstrates significant efficiency gains over the conventional local projections approach. It also shows robustness to high-dimensional controls. This application highlights the method’s practical use in empirical analysis, where high-dimensional confounders play a critical role.

Next, I reexamine the study by [Bhandari, Borovička, and Ho \(2024\)](#), which explores how subjective beliefs, particularly pessimism, influence macroeconomic aggregates like inflation and unemployment. The proposed method shows robustness even as model complexity increases, particularly when incorporating a moderate number of variables with extended lags. This robustness across varying model specifications is crucial in empirical analysis, where the true underlying model structure is often unknown. Furthermore, I introduce a novel state-dependent analysis that distinguishes between good and bad economic conditions. The results reveal that in good states, inflation follows a pattern consistent with the rational behavior of firms. In contrast, in bad states, inflation rises due to firms acting on subjective, pessimistic expectations of future costs. These state-dependent findings provide new insights into the role of belief shocks in shaping macroeconomic outcomes across different economic environments.

The remainder of this paper is organized as follows. Section 2 presents the notations and implementation details of the proposed method with two main applications for the identification schemes. Section 3 illustrates its finite sample performance through simulation studies. Section 4 outlines the theoretical framework, including definitions, assumptions, and main results. Section 5 presents two empirical applications: one examining the effect of democratization on GDP growth, and the other investigating the impact of pessimism on macroeconomic aggregates. Finally, Section 6 includes concluding remarks.

2 Overview of the Method

I will first introduce a general estimation framework and then provide further details on the estimation procedures in the latter part of this section. Consider the following h -step ahead local projection regression model

$$y_{t+h} = \beta_h x_t + \delta'_{h,0} \mathbf{r}_t + \sum_{\ell=1}^L \delta'_{h,\ell} \mathbf{z}_{t-\ell} + u_{t,h}, \quad (2.1)$$

where y_{t+h} is the h -step ahead response variable, x_t the innovation, \mathbf{r}_t are contemporaneous controls, and \mathbf{z}_t are lagged controls. The index $t = 1, \dots, \bar{T}$ is an index for the observations, $h = 1, \dots, H_{\max}$ is an index for horizons, and $\ell = 1, \dots, L$ is the number of lags included in the model. This is a general representation of local projections in the literature, as introduced in [Plagborg-Møller and Wolf \(2021\)](#). Following the spirit of [Jordà \(2005\)](#), I fix h and focus on each horizon of interest.

We are interested in the response of y_{t+h} with respect to a shock in x_t , and our parameter of interest β_h , is defined as

$$\beta_h = E \left[y_{t+h} | x_t = 1, \mathbf{r}_t, \{z_{t-\ell}\}_{\ell=1}^L \right] - E \left[y_{t+h} | x_t = 0, \mathbf{r}_t, \{z_{t-\ell}\}_{\ell=1}^L \right].$$

The parameter can be interpreted as impulse responses or treatment effects according to different identification assumptions. Below I introduce two applications which include the identification schemes.

2.1 Applications

Impulse response analysis with local projections

As was originally proposed by Jordà (2005), local projections are tools to estimate impulse responses with correctly specified controls. Plagborg-Møller and Wolf (2021) present a detailed review on how the LPs can be used to estimate the structural impulse responses, using their equivalence results between the VAR and LPs. I will briefly introduce this approach following Section 3.1. of Plagborg-Møller and Wolf (2021).

Denote the data as $w_t = (\mathbf{r}'_t, x_t, y_t, \mathbf{z}'_t)'$ with the dimension of \mathbf{r}_t as n_r . Consider the following Structural Vector Moving Average (SVMA) as the DGP

$$w_t = \mu + \Theta(L)\epsilon_t, \quad \Theta(L) = \sum_{\ell=0}^{\infty} \Theta_{\ell} L^{\ell},$$

and assume normality for the structural shocks: $\epsilon_t \stackrel{i.i.d.}{\sim} N(0, I_{n_{\epsilon}})$. Under some regularity conditions, the (i, j) th element of $\Theta_{i,j,h}$ is the impulse response of variable i -th element of w_t to the shock of j -th element of ϵ_t at horizon h . Consider the case where we are interested in the response of y_t with respect to a shock in $\epsilon_{1,t}$. The parameter of interest is then $\theta_h := \Theta_{n_r+2,1,h}$ for $h = 0, 1, \dots$.

Assuming that the structural shock can be recovered as a function of both current and past data, denoted as $\epsilon_{1,t} \in \text{span}(\{w_{\tau}\}_{\tau \leq t})$, the structural shock can be identified as a linear combination of the Wold forecast errors using an SVAR identification scheme. This can be expressed as $\tilde{\epsilon}_{1,t} = b'e_t$, where b is obtained as a function of reduced-form VAR parameters depending on identification schemes. The LP approach involves using reduced-form LP parameters instead of VAR counterparts to generate structural impulse responses. Using this method, the population estimand would be equivalent. For a detailed explanation

with different identification schemes, please refer to [Plagborg-Møller and Wolf \(2021\)](#).

In cases where the model is non-invertible, the straightforward approach would be to use instruments. I cannot efficiently deal with such cases since this paper does not provide a theory for the instrumental variable LP. However, as mentioned in [Känzig \(2021\)](#), non-invertibility is essentially the omitted variable bias problem. In that sense, I can argue that high-dimensional controls still help because the model spans more information.

The above results leverage the VAR-LP equivalence with infinite lags. In practical applications, we rely on a finite lag approximation. The use of finite lags introduces approximation errors, which must be carefully considered in empirical applications. A detailed discussion on the implications of using finite lags is provided in [Appendix C](#).

In the empirical analysis in [Section 5.2](#), I apply the impulse response analysis scheme outlined above to study the effects of subjective beliefs on some key economic aggregates. I consider several model specifications with an increasing number of lags, revisiting the issues of invertibility and finite lag approximations. This allows me to assess the robustness of the results to potential non-invertibility and to explore the trade-offs associated with different lag lengths in capturing the dynamic effects of belief shocks.

Local projections approach to difference-in-differences with high-dimensional controls

A recent paper by [Dube et al. \(2023\)](#) proposes a local projections approach to DiD event studies. Following their identification schemes, the parameter of interest β_h can be interpreted as a DiD estimator. In the following, I will briefly introduce their identification schemes with application to high-dimensional controls.

Consider a potential outcomes framework ([Rubin \(1974\)](#)) in a panel setting with a binary treatment. Denote $y_{it}(0)$ and $y_{it}(p)$ as the potential outcomes with respect to the control and treatment at time $p \neq \infty$ status. Units are divided into groups, $g \in \{0, 1, \dots, G\}$, where each group g shares the same treatment timing, p_g . Denote the group $g = 0$ as the never treated group with $p_0 = \infty$. Treatment is absorbing, meaning that once a unit receives treatment, it remains treated in all subsequent periods.

The group-specific average treatment effect on the treated (ATT) at horizon h for group g , which starts treatment at time p , is given by:

$$\tau_g(h) = E[y_{i,p+h}(p) - y_{i,p+h}(0) | p_i = p].$$

The DiD approach hinges on two main assumptions: parallel trends and no anticipation.

The no anticipation assumption implies that for any time t before the treatment time p , the expected difference in potential outcomes is ($E[y_{it}(p) - y_{it}(0)] = 0$). The parallel trend assumption states that $E[y_{i,t}(0) - y_{i,1}(0)|p_i = p] = E[y_{i,t}(0) - y_{i,1}(0)]$, for all $t \geq 2$ and for all $p \in \{1, \dots, T, \infty\}$. Also assume a simple structure to the never treated outcome to be

$$E[y_{i,t}(0)] = \alpha_i + \delta_t.$$

Now consider the following estimating equation.

$$y_{i,t+h} - y_{i,t-1} = \beta_h^{\text{LP-DiD}} \Delta D_{it} + \delta_t^h + e_{it}^h,$$

where δ_t^h are time specific controls and e_{it}^h the error terms. The LP-DiD parameter then identifies

$$\begin{aligned} E[\beta_h^{\text{LP-DiD}}] &= E[\Delta_h y_{it} | t, \Delta D_{it} = 1] - E[\Delta_h y_{it} | t, \Delta D_{it} = 0] \\ &= E \left[\sum_{g=1}^G (\tau_g(h) \times \mathbf{1}\{t = p_g\}) \right] \\ &\quad - E \left[\sum_{g=1}^G \left[\sum_{j=1}^{\infty} (\tau_g(h+j) - \tau_g(j-1)) \times \Delta D_{i,t-j} \times \mathbf{1}\{t = p_g + j\} \right] \right] \\ &\quad - E \left[\sum_{g=1}^G \left[\sum_{j=1}^{\infty} \tau_g(h-j) \times \Delta D_{i,t+j} \times \mathbf{1}\{t = p_g - j\} \right] \right], \end{aligned}$$

From this expression, we can clearly see the two bias terms. The contribution of the referenced paper is to restrict the sample such that both bias terms become zero.

The two key terms contributing to the biases $\Delta D_{i,t+j}$ for $j \leq h$ and $\Delta D_{i,t-j}$ for $1 \geq j$. These terms go to zero if $\Delta D_{i,t-j} = 0$ for $-h < j < \infty$, which simplifies to $D_{t+h} = 0$ under the assumption of absorbing treatment. This is where the sample restriction plays a critical role.

By restricting to the sample that are either

$$\begin{cases} \text{newly treated} & \Delta D_{it} = 1, \\ \text{or clean control} & D_{i,t+h} = 0, \end{cases}$$

the LP-DiD parameter identifies

$$\begin{aligned} E[\beta_h^{\text{LP-DiD}}] &= E[\Delta_h y_{it} | t, \Delta D_{it} = 1] - E[\Delta_h y_{it} | t, \Delta D_{it} = 0, D_{i,t+h}=0] \\ &= E\left[\sum_{g=1}^G (\tau_g(h) \times \mathbf{1}\{t = p_g\})\right], \end{aligned}$$

where it provides a convex combination of all group-specific effects $\tau_g(h)$ by removing previously treated observations and observations treated between $t + 1$ and $t + h$ from the control group.

Now, consider the scenario where the researcher believes the parallel trend holds only after controlling for a vector of covariates, \mathbf{w}_{it} . Including controls becomes necessary for the identification purpose, resulting in the following conditional parallel trend assumption:

$$E[y_{i,t}(0) - y_{i,1}(0) | p_i = p, \mathbf{w}_{it}] = E[y_{i,t}(0) - y_{i,1}(0) | \mathbf{w}_{it}].$$

The conditional parallel trends assumption becomes crucial when allowing for variations in outcome dynamics across different groups, provided that these differences can be fully accounted for by the covariates. This makes the assumption far more realistic than the conventional parallel trends assumption, especially in settings where untreated outcomes are not expected to evolve similarly across treatment groups. (Heckman et al., 1997; Abadie, 2005; Callaway and Sant'Anna, 2021).

Adopting my estimation framework introduces a new layer to this argument: by accounting for high-dimensional controls, the conditional parallel trends assumption becomes even more realistic and robust. By leveraging these controls, we ensure that any remaining variation in trends across groups is largely orthogonal to the treatment, further strengthening the identification strategy. This approach makes the conditional parallel trends assumption not only more plausible but also more applicable to modern datasets, where a wide range of observable factors can be accounted for in high-dimensional frameworks.

Then the estimating equation becomes

$$y_{i,t+h} - y_{i,t-1} = \beta_h^{\text{LP-DiD}^w} \Delta D_{i,t} + \mathbf{w}'_{i,t} \gamma^h + \delta_t^h + e_{i,t}^h,$$

where $\mathbf{w}_{i,t}$ can include lagged terms of the dependent variable and other controls. By restricting the sample to be newly treated group and the clean control group as before, the

LP-DiD^w parameter identifies

$$\begin{aligned} E[\beta_h^{\text{LP-DiD}^w} | \mathbf{w}_{it}] &= E[\Delta_h y_{it} | t, \Delta D_{it} = 1, \mathbf{w}_{it}] - E[\Delta_h y_{it} | t, \Delta D_{it} = 0, D_{i,t+h}=0, \mathbf{w}_{it}] \\ &= E\left[\sum_{g=1}^G (\tau_g(h) \times \mathbf{1}\{t = p_g\})\right]. \end{aligned}$$

This framework enables us to focus on the portion of outcome evolution that is not explained by the covariates, isolating the treatment effect more effectively. I will revisit this identification framework and its implications with the empirical application in Section 5.1.

2.2 Estimation Procedures

For notation simplicity, stack the covariates except for x_t into $\mathbf{w}_t = (r_t, z_{t-1}, \dots, z_{t-L})$ and write

$$y_{t+h} = \beta_h x_t + \beta'_{-h} \mathbf{w}_t + u_{t,h}, \quad (2.2)$$

where $\beta_{-h} = (\delta'_{h,0}, \delta'_{h,1}, \dots, \delta'_{h,L})'$. To address the bias that arises from excluding higher-order lag controls, the dimension of \mathbf{w}_t expands as the lag order, L , increases. Turning to the causal identification scheme of Angrist et al. (2018), it is intuitive to add a large set of covariates as controls to account for unobserved confounding variables, which also contributes to increasing the dimension of \mathbf{w}_t .

A straightforward approach to (2.2) with high dimensionality would be to apply a regularization method such as the LASSO. However, it is now well known that these methods come with an associated cost known as regularization bias. One way to address this challenge is a debiasing strategy using node-wise regression, regressing each covariate on the remaining covariates, as illustrated by Van de Geer, Bühlmann, Ritov, and Dezeure (2014) and Zhang and Zhang (2014). Using the estimates from the node-wise regressions, they construct a remedy for the bias term and control for it. An alternative approach is a double selection method that establishes an orthogonality condition in a similar spirit to Belloni et al. (2013). This method is analogous to the debiasing process of the LASSO, as noted in Semenova, Goldman, Chernozhukov, and Taddy (2023) and Chernozhukov, Härdle, Huang, and Wang (2021). In the context of (2.2), the main idea of both approaches is to incorporate another set of regressions of the covariates to control for the regularization bias, either by debiasing or by using the covariates selected in both regression models.

In this paper, I consider the double selection method with a model selection method OGA+HDAIC by Ing (2020), where it consists of two steps. OGA first orders the covariates \mathbf{w}_t by their explanatory power, and then we select the number of covariates that minimizes the high-dimensional AIC criteria. The selections come from the following regression models,

$$y_{t+h} = \lambda'_h \mathbf{w}_t + e_{t,h}, \quad (2.3)$$

$$x_t = \gamma'_h \mathbf{w}_t + v_{t,h}. \quad (2.4)$$

Although not necessary in (2.4), I used the subscript h for consistency across both equations. The concept involves applying OGA+HDAIC on both equations (2.3) and (2.4). To remove the regularization bias, I use the union of two selected covariates as \mathbf{w}_t to finally run the local projection regression in (2.2). For a clear presentation of the OGA+HDAIC procedure, I fix some notations below.

Notations. Let t be an index for observations and j for covariates, so that $\mathbf{w}_t = (w_{t,j})_{j=1}^p$ and $\mathbf{w}_j = (w_{t,j})_{t=1}^T$, where $p := \dim(\mathbf{w}_t)$ and $T := \bar{T} - h - L$ is the effective sample size. Let $[p] = 1, \dots, p$ be the set of all covariate indices. Let J be a set of covariate indices and let the subset of the covariates be $\mathbf{w}_t(J) := (w_{t,j})_{j \in J}$. Stack all $t = 1, \dots, T$ observations of $\mathbf{w}_t(J)$ and denote $W(J) := (\mathbf{w}_t(J))_{t=1}^T$. Similarly define $\mathbf{y}_h = (y_{t+h})_{t=1}^T$. Denote the projection matrix using $W(J)$ as $P_J := W(J)(W(J)'W(J))^{-1}W(J)'$.

First, consider the OGA part of y_{t+h} on \mathbf{w}_t . The ordering of the covariates requires the following definition, which indicates the explanatory power of the covariate \mathbf{w}_i .

$$\mu_i(\emptyset) = \frac{\mathbf{w}'_i \mathbf{y}_h}{\sqrt{T} \|\mathbf{w}_i\|} = \frac{\frac{1}{T} \mathbf{w}'_i \mathbf{y}_h}{\sqrt{\frac{1}{T} \mathbf{w}'_i \mathbf{w}_i}}, \quad (2.5)$$

As it looks, it works as a scaled version of a single regressor regression of \mathbf{y}_h on each regressor \mathbf{w}_i . Since it is scaled by the square root of the L_2 norm of each regressor, the scale of \mathbf{w}_i does not affect the magnitude of $\mu_i(J)$. To choose the one with the most explanatory power, we start with the setting $J = \emptyset$ and choose the one with the largest value of $|\mu_i(\emptyset)|$. Let this covariate index as

$$\hat{j}_1 := \arg \max_{i \in [p]} |\mu_i(\emptyset)|,$$

and define the first chosen set as $\hat{J}_1 := \{\hat{j}_1\}$. To select the second order covariate, we use the residuals from the first step, using $\mu_i(\hat{J}_1)$ to measure explanatory power. We choose the second order covariate from the remaining covariates, $\hat{j}_2 := \arg \max_{i \in [p] \setminus \hat{J}_1} |\mu_i(\hat{J}_1)|$, then update the chosen set of covariates, $\hat{J}_2 = \hat{J}_1 \cup \{\hat{j}_2\}$. Generalizing to the m -th order covariate, suppose we have the previously chosen set of covariates, \hat{J}_{m-1} . Compute the following coefficient for all $i \in [p] \setminus \hat{J}_{m-1}$, where

$$\mu_i(\hat{J}_{m-1}) = \frac{\mathbf{w}'_i(I - P_{\hat{J}_{m-1}})\mathbf{y}_h}{\sqrt{T} \|\mathbf{w}_i\|}, \quad (2.6)$$

and select the one with the largest absolute value of $\mu_i(\hat{J}_{m-1})$,

$$\hat{j}_m = \arg \max_{i \in [p] \setminus \hat{J}_{m-1}} |\mu_i(\hat{J}_{m-1})|, \quad (2.7)$$

and update the chosen set of covariates, $\hat{J}_m = \hat{J}_{m-1} \cup \{\hat{j}_m\}$. Repeating this procedure orders the covariates in descending order of their explanatory power, conditioning on the previously chosen set of covariates. Now that the covariates are ordered, the remaining task is to select the threshold for the number of covariates. The information criterion we use is HDAIC², defined as

$$\text{HDAIC}(J) = \left(1 + \frac{C^*|J| \log p}{T}\right) \hat{\sigma}_J^2, \quad (2.8)$$

where $\hat{\sigma}_J^2 = \mathbf{y}'_h(I - P_J)\mathbf{y}_h/T$. The number of covariates to be included in the model is the one which minimizes the information criteria,

$$\hat{m} = \arg \min_{1 \leq m \leq M_T^*} \text{HDAIC}(\hat{J}_m). \quad (2.9)$$

Denote the chosen set of covariates as $\hat{J}^{[1]} := \hat{J}_{\hat{m}}$. Next, repeat the OGA+HDAIC for (2.4) and obtain the set of covariates $\hat{J}^{[2]}$. Finally, denote the union set as $\tilde{J} = \hat{J}^{[1]} \cup \hat{J}^{[2]}$ and run

²Note that it is called HD because it takes into account the penalization on $\log p/T$. This notion, unlike the traditional AIC vs. BIC framework, takes into account the size of the entire feature space p relative to the available data T . This holistic approach to model complexity resonates in the high-dimensional setting, where the effect of the penalty is amplified as $\log p/T$ diverges with increasing dimensionality.

the local projection regression (2.2) with the selected covariates:

$$y_{t+h} = \beta_h x_t + \beta'_{-h} \mathbf{w}_t(\tilde{J}) + u_{t,h}.$$

The least squares estimator for β_h in this final model is our proposed estimator. For the variance estimator, define $\psi_t = v_{t,h} e_{t,h}$ and $\tau^2 = E[\sum_{t=1}^T v_{t,h}^2 / T]$. The variance estimator is then defined as

$$\hat{\sigma}_h^2 = \frac{1}{\hat{\tau}^2} \hat{\Omega}, \quad (2.10)$$

$$\hat{\Omega} = \sum_{\ell=-(K-1)}^{K-1} \left(1 - \frac{\ell}{K}\right) \frac{1}{T - \ell} \sum_{t=\ell+1}^T \hat{\psi}_t \hat{\psi}_{t-\ell}, \quad (2.11)$$

where $\hat{\Omega}$ is the Newey-West estimator with a bandwidth parameter K , which is assumed to be increasing with respect to increasing sample size. We borrow arguments from Andrews (1991) for the choice of K . $\hat{\psi}_t$ is the sample analogue of ψ_t , where $\hat{v}_{t,h}$ and $\hat{e}_{t,h}$ are the residuals from (2.3) and (2.4).

The proposed algorithm is detailed in Algorithm 1 after a remark on tuning parameters.

Remark. Unlike the OGA procedure, the HDAIC procedure has two unknown parameters, M_T^* and C^* . A detailed description of both definitions can be found in Appendix C. M_T^* is a parameter concerning the maximum number of covariates to include in the model and increases with $(T / \log p)$, as defined in (C.1). C^* , specified in (C.2), adjusts the penalty for dimensionality and is assumed to be greater than certain constants. While C^* could be viewed as a tuning parameter, it's more appropriately considered a hyperparameter, analogous to the hyperparameter of 2 in traditional AIC. Aside from the plug-in option, there is a data-driven way to choose the value of C^* by setting candidates, e.g. $\bar{C} = \{1.6, 1.8, 2, 2.2, 2.4\}$, and choosing the one that yields the smallest prediction errors in each regression in (2.3) and (2.4).

Algorithm 1. [Double-OGA+HDAIC]

1. Compute $\mu_i(\emptyset)$ in (2.5) for all $i \in [p]$ and select the covariate with the largest $|\mu_i(\emptyset)|$. Denote the index of covariate as \hat{j}_1 and define $\hat{J}_1 = \hat{j}_1$.
2. Given \hat{J}_1 , compute $\mu_i(\hat{J}_1)$ for all $i \in [p] \setminus \hat{J}_1$ and select the covariate with the largest $|\mu_i(\hat{J}_1)|$. Denote the index of covariate as \hat{j}_2 and define $\hat{J}_2 = \hat{J}_1 \cup \hat{j}_2$.

3. For $m > 2$, compute $\mu_i(\hat{J}_{m-1})$ for all $i \in [p] \setminus \hat{J}_{m-1}$ and select the covariate with the largest $|\mu_i(\hat{J}_{m-1})|$. Denote the index of covariate as \hat{j}_m and define $\hat{J}_m = \hat{J}_{m-1} \cup \hat{j}_m$.
4. Compute HDAIC in (2.8) and select m that minimizes $\text{HDAIC}(\hat{J}_m)$. Denote it as \hat{m}^y and define $\hat{J}_y := \hat{J}_{\hat{m}^y}$.
5. Run steps 1–4 by replacing y_{t+h} with x_t . Obtain \hat{J}_x and the residuals $\hat{v}_{t,h}$.
6. Run OLS of y_{t+h} on $[x_t : \mathbf{w}_t(\tilde{J})]$, where $\tilde{J} = \hat{J}_x \cup \hat{J}_y$. Obtain the final estimates $\hat{\beta}_h$ and the residuals $\hat{u}_{t,h} = y_{t+h} - \hat{\beta}_h x_t + \hat{\beta}'_{-h} \mathbf{w}_t(\tilde{J})$.
7. Calculate the variance estimator $\hat{\sigma}_h^2$ defined in (2.10).

With the above algorithm, one can construct an $100(1 - \alpha)\%$ confidence interval for h -step ahead impulse response estimator of the following form

$$[\hat{\beta}_h - z_\alpha \hat{\sigma}_h / \sqrt{T}, \hat{\beta}_h + z_\alpha \hat{\sigma}_h / \sqrt{T}],$$

where $z_\alpha = \Phi^{-1}(1 - \alpha/2)$ is the $(1 - \alpha/2)$ quantile of the standard normal distribution.

3 Illustrative Simulation Study

This section highlights the advantages of the proposed method over the commonly used LASSO approach, especially when dealing with unknown sparsity assumptions and the degree of persistence. I present a comparative analysis of the proposed estimator, the standard local projection estimator, and the debiased LASSO³, as described in Adamek et al. (2024). For the DGP, I adapt from Montiel Olea and Plagborg-Møller (2021). Consider the following DGP

$$\begin{aligned} y_{1,t} &= \rho y_{1,t-1} + u_{1,t}, \\ \mathbf{y}_t &= B_1 \mathbf{y}_{t-1} + \cdots + B_{12} \mathbf{y}_{t-12} + \mathbf{u}_t, \quad \mathbf{u}_t \sim N(0, \Sigma), \quad \Sigma_{i,j} = \tau^{|i-j|}, \end{aligned}$$

where $\mathbf{y}_t \in \mathbb{R}^n$. We are interested in estimating the reduced-form impulse response of $y_{2,t}$ with respect to the innovation $u_{1,t}$. I evaluate the finite sample properties with 95% coverage probabilities and the median widths of the confidence intervals over 1000 iterations.

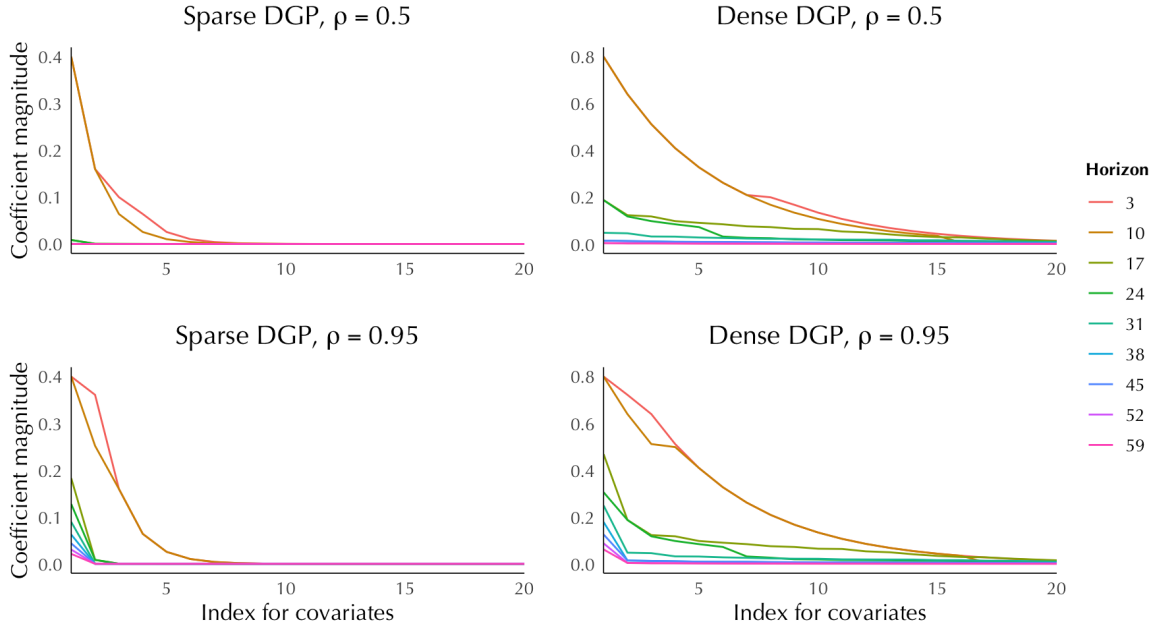
³For the debiased lasso estimation, I use the R package *desla* provided by Adamek et al. (2024).

For parameter settings, I set τ to be 0.3, $n = 10$, and I consider the sample size of $T = 300$. For estimation settings, I adopt the lag-augmentation and set the number of lags included in the model as $L = 21$, while the lags included in the DGP is 12. To evaluate performance over longer horizons, I estimate the reduced-form impulse responses for horizons from 1 to 60. The simulations explore different levels of persistence and sparsity by varying ρ and B_ℓ for $\ell = 1, \dots, 12$. Two levels of persistence are considered: $\rho = 0.5$ and $\rho = 0.95$. For sparsity, I define the values of B_ℓ using a vector $a \in \mathbb{R}^{n-1}$ of different magnitudes. I defined the even elements of each row $B^{\ell(j)}$ as polynomials of a_j with alternating signs. Different values of a are considered to generate different levels of sparsity, where I set $a^s = (0.4, -0.36, \dots, -0.094, 0.05)'$ for a sparse scenario and $a^d = (0.8, -0.73, \dots, -0.28, 0.2)'$ for a dense scenario.

The resulting coefficients of the corresponding local projection equations are depicted in Figure 1. The coefficients are ordered in descending order of their absolute magnitude. The left panel displays the regression coefficients from the local projection equation using the sparse vector a_s , while the right panel shows the coefficients using the dense vector a_d . The top panels correspond to data with lower persistence ($\rho = 0.5$), and the bottom panels correspond to data with higher persistence ($\rho = 0.95$). Each line represents the regression coefficients from the h -step ahead local projection equations, with horizons spanning from 3 to 59. Note that h ranges from 1 to 60, and I have selected 9 points within this range for illustration. In the left panel, the coefficients are sparse, with fewer than 10 coefficients being nonzero. In contrast, the right panel shows a dense set of coefficients; although the absolute magnitudes decay, a larger number of coefficients remain nonzero. The more persistent the data, the more amplified the largest ordered coefficients become.

Figures 2 and 3 show the simulation results for different levels of persistence. In the left panel of Figure 2, the model is sparse and the data are less persistent, making it easier for all estimation methods to perform well. Most methods achieve satisfactory coverage probabilities, except for debiased LASSO, which performs slightly worse. Notably, while the conventional LP achieves 95% coverage rates, it does so at the cost of significantly larger confidence interval widths compared to the high-dimensional methods. Additionally, the conventional LP method shows slight underperformance for the last 5 horizons, despite its large standard errors. This can be attributed to the sample size of $T = 300$ and the fact that the number of covariates included in the model is about 70% of the sample size. As a result, the standard error gets larger when fitting all covariates, and this issue worsens with increasing horizons due to the reduced effective sample size.

Figure 1: Magnitude of coefficients in the estimating equations



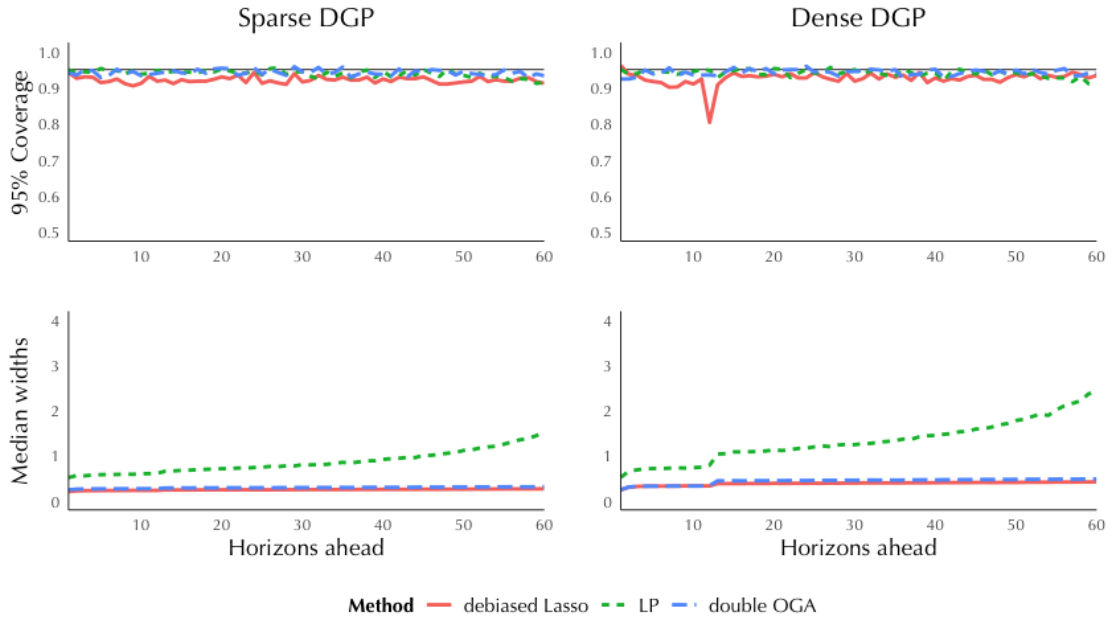
Notes. Each line represents h -step ahead local projection coefficients for horizons from 3 to 59. The coefficients are ordered in their absolute magnitudes. The left panel shows coefficients using the sparse vector a_s , while the right panel uses the dense vector a_d . The top panels are for lower persistence ($\rho = 0.5$) and the bottom panels for higher persistence ($\rho = 0.95$).

We can observe a similar pattern for the dense scenario in the right panel, except for a sharp failure in the initial horizons using the debiased LASSO method. The proposed method achieves the coverage rates with small standard errors across the different specifications. The huge gain in efficiency comes from the model selection, and it still achieves efficiency in the longer horizons. This is true for both high-dimensional methods.

Figure 3 presents the results for the higher persistence scenario. There is a huge failure of the debiased LASSO for either sparse or dense scenarios, especially when it gets to longer horizons. The reason for this failure can be inferred from the median width plot, where LASSO rules out too many regressors. The conventional LP performs similarly to the less persistent case, where it achieves the coverage rates but with larger standard errors. Overall, the proposed method maintains the coverage rates at a much lower cost compared to the conventional LP.

The simulation results illustrate that the proposed method maintains desirable coverage rates with more stable and narrower confidence intervals across different specifications. While the conventional LP also achieves the coverage probabilities, it suffers from larger

Figure 2: 95% Coverage probabilities and median widths, less persistent case



Notes. The figure compares 95% coverage probabilities (top panels) and median widths (bottom panels) over 60 forecast horizons for sparse and dense DGPs, generated with a_s (left panels) and a_d (right panels) in the less persistent case ($\rho = 0.5$). The results are based on 1,000 iterations. The red solid line represents the debiased Lasso method, the green dotted line indicates conventional LP, and the blue dashed line corresponds to the proposed method.

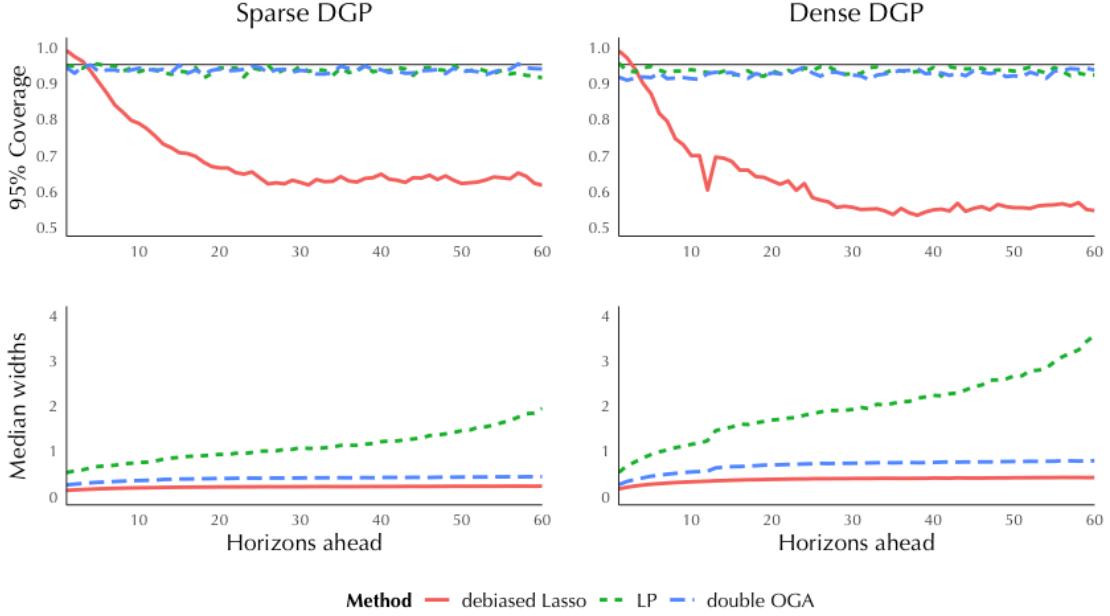
standard errors, especially as the horizon increases. As the debiased LASSO consistently gives the smallest standard errors throughout all scenarios, there might be an appropriate DGP where it outperforms the proposed method at least in terms of efficiency, but less likely in dense scenarios, as the performance of debiased LASSO tends to decline with denser DGPs. Given the uncertainties regarding the underlying sparsity and persistence of the data, the proposed method provides a robust and reliable alternative that performs well across various conditions.

4 Theory

4.1 Preliminaries

In this subsection, I introduce the definitions used throughout the theory. Most of the definitions and explanations are taken from Davidson (2021). I will use these definitions in

Figure 3: 95% Coverage probabilities and median widths, more persistent case



Notes. The figure compares 95% coverage probabilities (top panels) and median widths (bottom panels) over 60 forecast horizons for sparse and dense DGPs, generated with a_s (left panels) and a_d (right panels) in the less persistent case ($\rho = 0.95$). The results are based on 1,000 iterations. The red solid line represents the debiased Lasso method, the green dotted line indicates conventional LP, and the blue dashed line corresponds to the proposed method.

the context of the main text in the following subsection.

Consider a probability space (Ω, \mathcal{F}, P) . With time series data, time flows in one direction: The past is known while the future is unknown. It is hence important to condition on previous information set in the context of time series analysis. The accumulation of information is represented by an increasing sequence of sub σ -fields, $\{\mathcal{F}_t\}_{-\infty}^{\infty}$, where $\mathcal{F}_s \subseteq \mathcal{F}_t$ for $s \leq t$. With the uncertainty of the future, the natural next step is to take expectations. If X_t is \mathcal{F}_t -measurable for each t , $\{X_t, \mathcal{F}_t\}_{-\infty}^{\infty}$ is called an adapted sequence, and $E[X_t | \mathcal{F}_{t-1}]$ is defined. Also, if $E[X_{t+s} | \mathcal{F}_t] = X_t$ a.s. for all $s \geq 0$ under adaptation, the sequence is identified by its history alone, and $\{X_t\}_{-\infty}^{\infty}$ is called a causal stochastic sequence. I start by introducing the most widely used dependence concept, the martingale difference (m.d.) sequences.

Definition 1 (Martingale difference sequence, Davidson (2021)). The process $\{X_t\}_{-\infty}^{\infty}$ is a

martingale difference sequence if

$$\begin{aligned} E[X_t] &< \infty \\ E[X_t | \mathcal{F}_{-\infty}^{t-1}] &= 0 \quad a.s. \end{aligned}$$

As is clear from the definition, m.d. assumes one-step-ahead unpredictability. It follows that it is uncorrelated with any measurable function of its lagged values, and thus behaves like independent sequences in classical limit results. As shown in [Davidson \(2021\)](#), many limit theorems that hold under independence also hold under the m.d. assumption with few additional assumptions about the marginal distributions, making it a preferred dependence assumption for econometricians. To extend our understanding beyond one-step-ahead unpredictability, the next definition introduces the concept of asymptotic unpredictability.

Definition 2 (Mixingale, [Davidson \(2021\)](#)). For $q \geq 1$, the sequence $\{X_t, \mathcal{F}_t\}_{-\infty}^{\infty}$ is an L_q -mixingale if for a sequence of non-negative constants $\{c_t\}_{-\infty}^{\infty}$ and $\{\rho_m\}_0^{\infty}$ such that $\rho_m \rightarrow 0$ as $m \rightarrow \infty$,

$$\left(E \left[|E[X_t | \mathcal{F}_{-\infty}^{t-m}]|^q \right] \right)^{1/q} \leq c_t \rho_m, \quad (4.1)$$

$$\left(E \left[|X_t - E[X_t | \mathcal{F}_{-\infty}^{t+m}]|^q \right] \right)^{1/q} \leq c_t \rho_{m+1}, \quad (4.2)$$

hold for all t and $m \geq 0$.

A mixingale generalizes a m.d. as a special case where $\rho_m = 0$ for all $m > 0$. The equations show a diminishing effect of past information on the present, while suggesting eventual complete knowledge of the present in the distant future. Note that if the sequence is adapted, then $E[X_t | \mathcal{F}_{-\infty}^{t+m}] = X_t$ for all $m \geq 0$ and (4.2) is satisfied. Just as m.d.s behave like independent sequences in limit theorems, mixingales behave like mixing sequences, which implies asymptotic independence with the following definitions.

Definition 3 (α -mixing coefficients, [Hansen \(1991\)](#)). The α -mixing coefficients of a sequence $\{X_t\}_{-\infty}^{\infty}$ are given by

$$\alpha_m = \sup_j \sup_{\{F \in \mathcal{F}_{-\infty}^j, G \in \mathcal{F}_{j+m}^{\infty}\}} |P(G \cap F) - P(G)P(F)|,$$

and the process X_t is said to be α -mixing if $\lim_{m \rightarrow \infty} \alpha_m = 0$.

The α -mixing coefficient α_m measures the dependence between the sequences separated by a lag of m . If a process X_t is α -mixing, the dependence diminishes as the lag increases. Mixing conditions often play a crucial role in further establishing asymptotic properties. Although the mixingale condition offers several advantageous properties, an important limitation arises: even if a function of mixingales is independent, it loses its mixing property with an infinite number of lags (Davidson (2021), Chapter 18). The following definition introduces a mapping from a mixing process to a random sequence. This transformation enables the sequence to inherit some desired mixingale properties.

Definition 4 (Near Epoch Dependence (NED), Davidson (2021)). For a stochastic process $\{V_t\}_{-\infty}^{\infty}$, let $\mathcal{F}_{t-m}^t = \sigma\{V_{t-m}, \dots, V_t\}$, such that $\{\mathcal{F}_{t-m}^t\}_{m=0}^{\infty}$ is an increasing sequence of σ -fields. If for $q > 0$ an adapted sequence $\{X_t\}_{-\infty}^{\infty}$ satisfies

$$\left(E \left[|X_t - E(X_t | \mathcal{F}_{t-m}^t)|^q \right] \right)^{1/q} \leq d_t \zeta_m, \quad (4.3)$$

where $\zeta_m \rightarrow 0$ as $m \rightarrow \infty$ and $\{d_t\}_{-\infty}^{\infty}$ is a sequence of positive constants, X_t is said to be near-epoch dependent in L_q -norm (L_q -NED) on $\{V_t\}_{-\infty}^{\infty}$.

The NED condition is the main dependence assumption I use on the data, following Adamek et al. (2023) and Adamek et al. (2024). In the rest of the subsection, I introduce some useful lemmas using the aforementioned definitions.

The following lemma gives a concentration bound without a specific assumption on the dependence structure, which will be used both in Theorems 4.1 and 4.3.

Lemma 4.1 (Triplex inequality, Jiang (2009)). Let $\{X_t\}_{-\infty}^{\infty}$ be a causal stochastic sequence and $\{\mathcal{F}_{t-m}^t\}_{m=0}^{\infty}$ be an increasing sequence of σ -fields. Let $\{X_t\}$ be \mathcal{F}_t -measurable for each t . Then for any $\epsilon, M > 0$ and positive integers m ,

$$\begin{aligned} P \left(\left| \frac{1}{T} \sum_{t=1}^T X_t - EX_t \right| > \epsilon \right) &\leq 2m \exp \left(-\frac{T\epsilon^2}{288m^2M^2} \right) \\ &+ (6/\epsilon) \frac{1}{T} \sum_{t=1}^T E[E[X_t | \mathcal{F}_{t-m}^t] - EX_t] \\ &+ (15/\epsilon) \frac{1}{T} \sum_{t=1}^T E[|X_t| \mathbb{1}\{|X_t| > M\}] \end{aligned} \quad (4.4)$$

This inequality is called the triplex inequality because it has three components. The first element is a Bernstein-type bound, the second deals with dependence, and the last

component is on the tail. This bound is a central theory used in the proofs, where I use the mixingale property inherited by the NED assumption to simplify the dependence and the tail bounds. The following lemma provides the simplified bounds by imposing the mixingale assumptions on $\{X_t\}_{-\infty}^{\infty}$.

Lemma 4.2 (Triplex inequality for mixingales). *Suppose the assumptions in Lemma 4.1 hold. Further assume that the moment generating function for X_t exists and $\{X_t\}_{-\infty}^{\infty}$ is an $L_{\bar{q}}$ -bounded L_q -mixingale with constants c_t and $\rho_m \rightarrow 0$ for some $1 \leq \bar{q} \leq q$, so that $E[|X_t|^{\bar{q}}] \leq C$. Then for any $\epsilon, M > 0$ and positive integers m ,*

$$P\left(\left|\frac{1}{T}\sum_{t=1}^T X_t - EX_t\right| > \epsilon\right) \leq 2m \exp\left(-\frac{T\epsilon^2}{288m^2M^2}\right) + \frac{6\bar{c}_T}{\epsilon}\rho_m + \frac{15}{\epsilon}C \exp(-M(\bar{q}-1)), \quad (4.5)$$

where $\bar{c}_T := \sum_{t=1}^T c_t / T$.

Proof. The proof can be found in Appendix B.1. □

4.2 Assumptions and Lemmas

The definitions of the variables and the parameters come from the baseline models (2.2) – (2.4). I start by introducing the assumptions on the data generating processes.

Assumption 1 (NED). *Denote $\epsilon_{t,h}$ as a generic notation for the error terms $u_{t,h}$, $e_{t,h}$, and $v_{t,h}$. There exist some constants $\bar{q} > q > 2$, and $b \geq \max\{1, (\bar{q}/q - 1)/(\bar{q} - 2)\}$ such that*

- (a) $(x_t, \mathbf{w}_t, u_{t,h}, e_{t,h})$ are zero-mean causal stochastic process with $E[x_t u_{t,h}] = E[x_t e_{t,h}] = 0$ and $E[\mathbf{w}_t u_{t,h}] = E[\mathbf{w}_t e_{t,h}] = \mathbf{0}$.
- (b) $\max_{1 \leq j \leq p} E[|w_{t,j}|^{2\bar{q}}] \leq C$ and $\max_{1 \leq h \leq H_{\max}} E[|\epsilon_{t,h}|^{2\bar{q}}] \leq C$.
- (c) Denote the moment generating function of X as $M_X(t)$. Assume $M_X(t) < \infty$ for $X = \{w_{t,j}, \epsilon_{t,h}, w_{t,j}, w_{t,k}\}$ for all $j, k = 1, \dots, p, j \neq k$.
- (d) Let $\{Y_{T,t}\}$ denote a triangular array that is α -mixing of size $-b/(1/q - 1/\bar{q})$ with σ -field $\mathcal{F}_t^Y := \sigma\{Y_{T,t}, Y_{T,t-1}, \dots\}$ such that $(x_t, \mathbf{w}_t, u_{t,h}, e_{t,h})$ is \mathcal{F}_t^Y -measurable. The processes $x_t, w_{t,j}, u_{t,h}$, and $e_{t,h}$ are L_{2q} -near-epoch-dependent (NED) of size $-b$ on $Y_{T,t}$ with positive constants $\{d_t\}$ and a sequence $\zeta_m \rightarrow 0$ as $m \rightarrow \infty$, uniformly over $j = 1, \dots, p$.

Assumption 1 (a) assumes that the error terms in (2.2) and (2.3) are not correlated with the contemporaneous regressors. Note that I impose the adaptation assumption to use asymptotic martingale difference property the Bernstein blocks must have (Davidson (1994), page 387). According to Davidson (2021), it is a widely employed assumption in time series econometrics, assuming that future shock information cannot help in predicting X_t given its history (Davidson (2021), page 383). Assumption 1 (b) ensures the processes have bounded $2\bar{q}$ -th moments. Assumption 1 (d) is on the dependence structure. While $(x_t, w_t, u_{t,h}, e_{t,h})$ themselves are not mixing processes, they depend almost entirely on ‘near epoch’ of $\{Y_t\}$ (Davidson (2021), page 368), which is α -mixing. This allows $(x_t, w_t, u_{t,h}, e_{t,h})$ to inherit some mixingale properties, as will be stated in the following lemma.

Lemma 4.3 (Mixingale Property). *Denote $\epsilon_{t,h}$ as a generic notation for the error terms $u_{t,h}, e_{t,h}$, and $v_{t,h}$. Under Assumption 1, the following holds. Note that $\{c_t\}$ and ρ_m are generic notations for the mixingale constants.*

- (a) $\{v_{t,h}\}_{t=-\infty}^{\infty}$ is causal $L_{2\bar{q}}$ -NED of size $-b$ on $Y_{T,t}$ with positive bounded constants uniformly over $h = 1, \dots, H_{\max}$.
- (b) $\{w_{t,j}\epsilon_t\}$ is a causal L_q -mixingale with non-negative constants $\{c_t\}$ and sequences ρ_m for all $j = 1, \dots, p$ and $h = 1, \dots, H_{\max}$.
- (c) $\{w_{t,j}w_{t,k} - E[w_{t,j}w_{t,k}]\}$ is a causal L_q -mixingale with non-negative constants $\{c_t\}$ and sequences ρ_m for all $j \neq k$ where $j, k = 1, \dots, p$.

Proof. The proof can be found in Appendix B.2. □

This lemma shows that some transformations of NEDs and their demeaned processes are mixingales. It thus allows us to use Lemma 4.2. Next, I impose some assumptions on the mixingale constants to simplify some bounds used in the proof of the main theorems.

Assumption 2. *Recall the NED constants $\{d_t\}$ and a sequence $\zeta_m \rightarrow 0$ defined in Assumption 1 (d). Let $\tilde{\zeta}_m = 2\zeta_m + \zeta_m^2$ and $k := \lceil q/2 \rceil$. Define $\rho_m = 6\alpha_k^{1/q-1/\bar{q}} + 2\tilde{\zeta}_k$, where α_k is the mixing coefficient for the sequences $X = \{\epsilon_{t,h}, v_{t,h}, w_{t,j}\epsilon_{t,h}, w_{t,j}w_{t,k}\}$ for all $j = 1, \dots, p$ and $h = 1, \dots, H_{\max}$. Assume that*

$$\rho_m \leq \exp(-m\kappa)$$

for some $\kappa > c_\kappa \log p$, where $c_\kappa > 2$.

This assumption is on the mixingale constants, where I define the constants to align with the constants that inherit the mixingale properties. The sequence $\rho_m \rightarrow 0$ is hence the mixingale sequence for the transformed variables in Lemma 4.3. Assumption 2 gives the assumption of how fast ρ_m should decay. The parameter κ governs the strength of the dependence, with larger κ values indicating a weaker dependence. Note that this is a technical assumption I need to prove Theorem 4.1, where it simplifies the dependence bound in the triplex inequality (4.4). The following is the assumptions on the degree of sparseness of the underlying coefficients, λ_h and γ_h .

Assumption 3. Let $|\beta_h| \leq C$. Let ξ be a generic notation that represents β_{-h} , λ_h , and γ_h for all $h = 1, \dots, H_{\max}$. Then ξ follows the following assumption. Suppose $\sum_{j=1}^p \xi_j^2 \leq C$. Also assume that there exists $\delta > 1$ and $0 < C_\delta < \infty$ that for any $J \subseteq \mathfrak{P}$,

$$\sum_{j \in J} |\xi_j| \leq C_\delta \left(\sum_{j \in J} \xi_j^2 \right)^{(\delta-1)/(2\delta-1)}, \quad (4.6)$$

where C refers to a generic constant $0 < C < \infty$. \mathfrak{P} refers to the power set of J , where J is a set of covariates.

This assumption is the main difference between this method and LASSO, in that it doesn't limit the number of nonzero coefficients, but rather restricts the magnitudes of the coefficients. While we do not require that the parameters to have a natural order, these conditions can be expressed more simply by rearranging the parameters in descending order of their magnitude $|\xi_j|$. Denote the rearrangement as $|\xi_{(1)}| \geq |\xi_{(2)}| \geq \dots \geq |\xi_{(p)}|$. Then, Assumption 3.3 implies

$$C_1 j^{-\delta} \leq |\xi_{(j)}| \leq C_2 j^{-\delta}, \quad 0 < C_1 \leq C_2 < \infty, \quad \delta > 1, \quad (4.7)$$

where from (4.7) we call Assumption 3.3 as a polynomial decay case: if (4.7) holds for some $\delta > 1$, then (4.6) holds for the same δ , as shown in Lemma A.2 in Ing (2020). Apart from (4.7), it can be shown that Assumption 3.3 also implies

$$\sum_{j=1}^p |\xi_j|^{1/\delta} < C, \quad 0 < C < \infty, \quad \delta > 1, \quad (4.8)$$

which is a frequently adopted assumption in the high-dimensional literature, as in Wang, Paterlini, Gao, and Yang (2014). Assume that (4.8) holds for some δ . Applying Hölder's

inequality,

$$\begin{aligned}
\sum_{j \in J} |\tilde{\zeta}_j| &\leq \left(\sum_{j \in J} |\tilde{\zeta}_j|^{\frac{1}{2\delta-1} \frac{2\delta-1}{\delta}} \right)^{\delta/(2\delta-1)} \left(\sum_{j \in J} \tilde{\zeta}_j^{\frac{2\delta-2}{2\delta-1} \frac{2\delta-1}{\delta-1}} \right)^{(\delta-1)/(2\delta-1)} \\
&= \left(\sum_{j \in J} |\tilde{\zeta}_j|^{1/\delta} \right)^{\delta/(2\delta-1)} \left(\sum_{j \in J} \tilde{\zeta}_j^2 \right)^{(\delta-1)/(2\delta-1)} \\
&\leq C^{\delta/(2\delta-1)} \left(\sum_{j \in J} \tilde{\zeta}_j^2 \right)^{(\delta-1)/(2\delta-1)},
\end{aligned}$$

and we can see that by setting $C_\delta = C^{\delta/(2\delta-1)}$, (4.6) holds. The parameter δ governs the degree of sparseness, with larger values indicating a faster decay of the coefficients. Thus, we can see that Assumption 3 covers a wider class of sparsity conditions where the condition trivially implies the exact sparsity case.

Remark. There are many variations of sparsity-based assumptions that extend the exact/strong sparse assumption. First, (4.8) is called a soft sparsity, as opposed to strong sparsity, in that L_q norm is bounded for $0 < q \leq 1$, whereas strong sparsity means that L_0 norm is bounded by a small constant. Another concept is the approximate sparsity (Chernozhukov et al. (2021), Comment 3.1). The concept is to add a fast enough approximation error based on the error bounds, so that exact sparsity can “approximate” a less sparse DGP such as (4.7).

Assumption 4. Assume the followings.

(a) For some positive constant C_1 and C_2 , it holds that

$$\max_{1 \leq |J| \leq C_1 (T/\log p)^{1/2}, i \notin J} \left\| \Gamma^{-1}(J) E[\mathbf{w}_{t,i} \mathbf{w}_t(J)] \right\|_1 < C_2,$$

where $\Gamma(J) = E[\mathbf{w}_t(J) \mathbf{w}_t(J)']$.

(b) Let $\Sigma = E[\sum_{t=1}^T \mathbf{w}_t \mathbf{w}_t' / T]$. Assume $\max_{j \in [p]} \Sigma_{j,j} < C$ and $1/C \leq \Lambda_{\min}$, where Λ_{\min} is the minimum eigenvalue of Σ and $0 < C < \infty$.

(c) $\log p = o(T^{\frac{\delta-1}{3(2\delta-1)}})$ and $(T/(\log p)^3)^{1/2} p^{-\underline{c}} = o(1)$ for some $\underline{c} = \min\{c_\kappa - 2, c_M(\bar{q} - 1) - 2\} > 0$, where $c_M > 2/(\bar{q} - 1)$ and $c_\kappa > 2$.

Assumption 4 are some additional assumptions on the covariates and growth rates of the dimensionality $\dim(\mathbf{w}_t) = p$. Assumption 4 (a) limits strong correlations between covariates, ensuring that the OLS coefficients of one covariate on any set of other covariates remain finite. Assumption 4 (b) is on minimum eigenvalue of the Gram matrix, with a remark that this condition is on the population level, not on the sample matrix as in the restricted eigenvalue conditions in [Bickel, Ritov, and Tsybakov \(2009\)](#). The third condition addresses the relationship between the growth of the covariate dimension p and sample size T . It specifies that $\log p$ should not grow too quickly compared to T . This condition is crucial for bounding the triplex inequality in the proof of [Theorem 4.1](#). Note that this assumption is stronger than the usual growth rates in the high-dimensional literature with i.i.d. data, for example $\log p = o(T^{1/3})$ in [Belloni et al. \(2013\)](#). While bounding either the Bernstein bound or the tail bound would require $\log p = o(T^{(\delta-1)/(2\delta-1)})$, bounding all the terms simultaneously requires a stricter condition $(\log p)^3 = o(T^{(\delta-1)/(2\delta-1)})$. More detailed explanations are given in the proofs of [Theorems 4.1](#) and [4.2](#). While this may sound restrictive, note that this assumption is on the growth rate of $\log p$, where p can grow at much faster rates.

4.3 Inference

In this subsection I establish the inference for the parameter of interest with each horizon h . I use a matrix representation as the baseline instead of [\(2.2\) – \(2.4\)](#) for simplicity. Let \mathbf{y}_h , \mathbf{x}_h , \mathbf{u}_h , and \mathbf{v}_h be the $T \times 1$ vector and W_h be the $T \times p$ matrix, where $p = \dim(\mathbf{w}_t)$. Then the models can be written in a compact matrix form:

$$\begin{aligned}\mathbf{y}_h &= \beta_h \mathbf{x}_h + W_h \beta_{-h} + \mathbf{u}_h, \\ \mathbf{x}_h &= W_h \gamma_h + \mathbf{v}_h.\end{aligned}\tag{4.9}$$

Theorem 4.1 (Error bounds for Double OGA+HDAIC). *Denote ξ as a representative vector of parameters, β_{-h} and γ_h , for all $h = 1, \dots, H_{\max}$. Denote $E_T[\cdot] = E[\cdot | (y_{t+h}, x_t, \mathbf{w}_t)_{t=1}^{T-h}]$. Under [Assumptions 1 – 4](#), the following holds for all $h = 1, \dots, H_{\max}$.*

$$E_T \left[\left\| W_h (\hat{\xi} - \xi) \right\|^2 \right] = O_p \left(\left(\frac{(\log p)^3}{T} \right)^{1-1/2\delta} \right).\tag{4.10}$$

Proof. The proof can be found in [Appendix A.1](#). □

Note that the convergence rates are not the fastest rates proposed in the main theorem in Ing (2020): the error bounds are $(\log p/T)^{1-1/2\delta}$ for the polynomial decay case. The main results require assumptions (A1) and (A2) in Ing (2020), and with Assumption 1 and Lemma 4.2 those assumptions are not satisfied. I hence use the bounds from weakened assumptions in equations (2.33) and (2.34) in Ing (2020), resulting in the slower converge rates. As noted in equation (2.35) of Ing (2020), these relaxed assumptions require $\log p = o(T^{1/3})$, which is implied by Assumption 4 (c). While Theorem 4.1 itself is useful in deriving error bounds for the high-dimensional nuisance parameters, our parameter of interest is β_h in equation (2.2). The following theorem derives asymptotic distribution of $\hat{\beta}_h$ using the error bounds derived in Theorem 4.1.

Theorem 4.2. *Under Assumptions 1 – 4,*

$$\sqrt{T}(\hat{\beta}_h - \beta_h) \xrightarrow{d} N(0, \sigma_h^2),$$

where $\sigma_h^2 = \lim_{T \rightarrow \infty} \Omega_h / \tau_h^4$, Ω_h is the long-run covariance matrix following Newey-West, and $\tau^2 = E[\mathbf{v}'_h \mathbf{v}_h / T]$.

Proof. The proof can be found in Appendix A.2. □

By Theorem 4.2, the estimator of interest achieves the square root T convergence rate regardless of the slower convergence rate of the nuisance parameters presented in Theorem 4.1. The following theorem establishes the validity of the proposed variance estimator.

Theorem 4.3. *Define $\psi_{h,t} = v_{h,t}u_t$ and $\tau_h^2 = E[\mathbf{v}_h \mathbf{v}_h / T]$. Let $\sigma_h^2 = \lim_{T \rightarrow \infty} \tau_h^{-4} \Omega_h$, where $\Omega_h = \sum_{\ell=-T}^{T-1} 1/T \sum_{t=\ell+1}^T E[\psi_{h,t} \psi_{h,t-\ell}]$ with a bandwidth parameter K . Denote the sample analogues as $\hat{\tau}_h$, $\hat{\sigma}_h^2$ and $\hat{\Omega}_h$. Under Assumptions 1 – 4,*

$$\left| \hat{\sigma}_h^2 - \sigma_h^2 \right| \xrightarrow{p} 0.$$

Proof. The proof can be found in Appendix A.3. □

With Theorems 4.2 and 4.3, we can now construct $100(1 - \alpha)\%$ confidence intervals for each horizon. Given a confidence level α , an asymptotic $100(1 - \alpha)\%$ confidence interval $\hat{\mathcal{I}}_{\alpha,h}$ is given by

$$\hat{\mathcal{I}}_{\alpha,h} := [\hat{\beta}_h - z_\alpha \hat{\sigma}_h / \sqrt{T}, \hat{\beta}_h + z_\alpha \hat{\sigma}_h / \sqrt{T}], \quad (4.11)$$

where $z_\alpha = \Phi^{-1}(1 - \alpha/2)$ is the $(1 - \alpha/2)$ quantile of the standard normal distribution and $\hat{\sigma}_h$ is defined in Theorem 4.2.

5 Empirical Applications

5.1 The Effect of Democracy on GDP

I illustrate the performance of the proposed method through an empirical investigation of the response of GDP growth to democratization, revisiting the LP framework in Acemoglu et al. (2019). They develop a binary index of democracy by gathering information from several different sources of data. The data covers 184 countries from 1960 to 2010. In part of their analysis, they adopt the LP specification to see how the effect of democratization evolves over time. I adopt the baseline LP specification in Acemoglu et al. (2019)

$$y_{c,t+h} - y_{c,t-1} = \beta_h^{\text{LP-DiD}} \Delta D_{ct} + \delta_t^h + \sum_{j=1}^p \gamma_j^h y_{c,t-j} + \epsilon_{ct}^h, \quad (5.1)$$

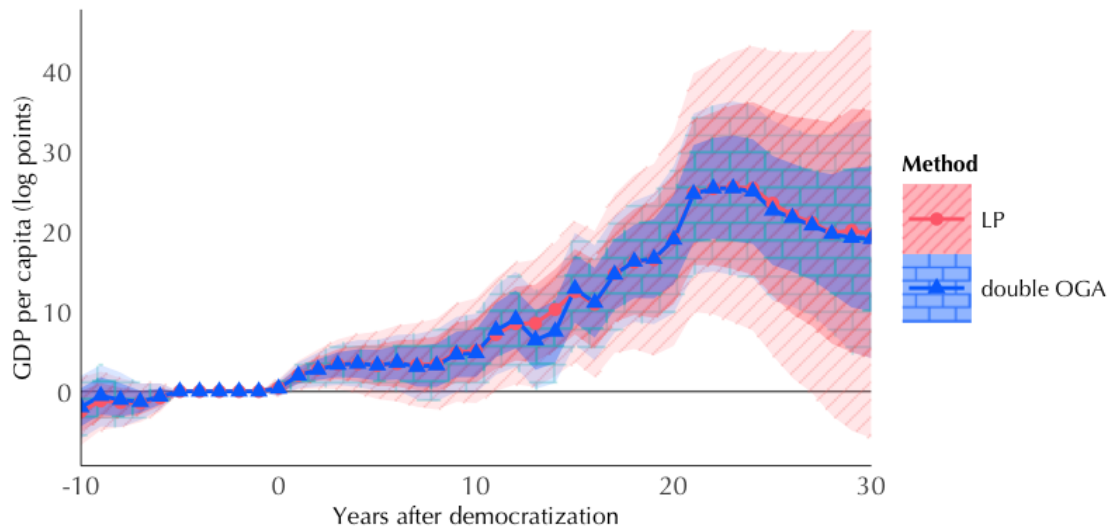
where $y_{c,t}$ denotes the log GDP per capita in country c at time t , D_{ct} is the binary democracy variable, and δ_t^h the time dummy. The baseline model includes the lagged terms of the GDP to address the selection into democracy, as the descriptive data suggests the dip in GDP preceding democratizations. The identifying assumption is that conditional on the lags of GDP, countries that democratize do not follow a different GDP trend relative to other nondemocracies. This specification can be viewed as a version of the LP-DiD identification scheme by Dube et al. (2023), where the sample is restricted to

$$\begin{cases} \text{democratizations} & D_{it} = 1, D_{i,t-1} = 0 \\ \text{clean controls} & D_{it} = D_{i,t-1} = 0. \end{cases}$$

I ran (5.1) with the conventional LP and with my method, with $p = 4$ lags of $y_{c,t}$ included as controls. The results are depicted in Figure 4. While the point estimates are very similar, the proposed method has efficiency gain overall, especially for the logner horizon estimates. As expected, the standard errors increase with the horizon due to the decreasing effective sample size. However, even after accounting for long-run variance, the proposed method results in smaller standard errors, attributable to the model selection process. The empirical findings align with the original results, indicating significant GDP growth of 20

percent higher than the controls over a 20-year period.

Figure 4: The effect of democratization on GDP growth, baseline model



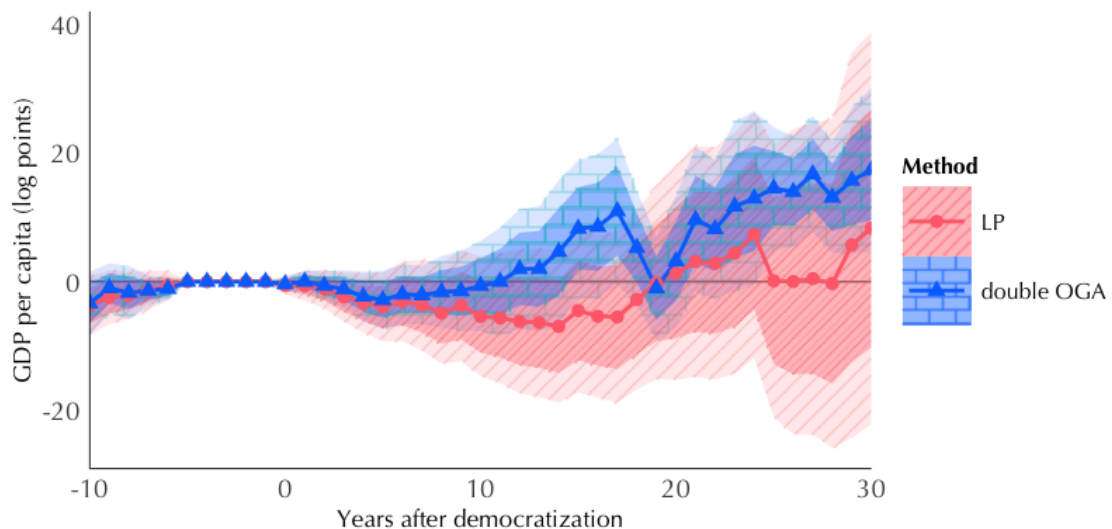
Notes. This model follows the baseline model in (5.1), where 4 lags of GDP are included as controls. Solid lines represent the point estimates, derived using the LP (red, diagonal shading) and double OGA (blue, brick-shaped shading) methods. Light-shaded areas indicate 90% confidence intervals; dark shades 68%.

However, as noted in their paper, even after controlling for fixed effects and GDP dynamics, there are possible sources of bias coming from unobservables related to future GDP and the change in democracy. To investigate these factors, the authors show the robustness of the results with different sets of controls. The sets of controls include potential trends related to differences in the level of GDP in the initial period, dummies for the democracy of Soviet and Soviet satellite countries, lags of trade and financial flows, lags of demographic structure, and the full set of $\text{region} \times \text{initial regime} \times \text{year}$ dummies, and more in the appendix. To see the robustness against high-dimensional controls, I have combined these controls into a union set. This brings the number of covariates included in the model to 276 with a sample size of 774.

The results are displayed in Figure 5. As expected for the conventional LP, the standard errors are larger due to the inclusion of all regressors, and the estimates are generally insignificant. Even with the proposed method, most estimates remain insignificant, although it manages to maintain moderate standard errors. However, the proposed method identifies significant GDP growth at longer horizons, starting from year 25 onward. The percentage increase reaches 17.33 percent in year 30, which is consistent with the original

findings using baseline controls. This result suggests that the proposed method provides reliable estimates even when considering a large number of potential confounders, which is essential for the causal interpretation of the parameter.

Figure 5: The effect of democratization on GDP growth, high-dimensional controls



Notes. The model includes a total of 276 covariates, which are listed in the main text. Solid lines represent the point estimates, derived using the LP (red, diagonal shading) and double OGA (blue, brick-shaped shading) methods. Light-shaded areas indicate 90% confidence intervals; dark shades 68%.

5.2 Subjective Beliefs in Business Cycle Models

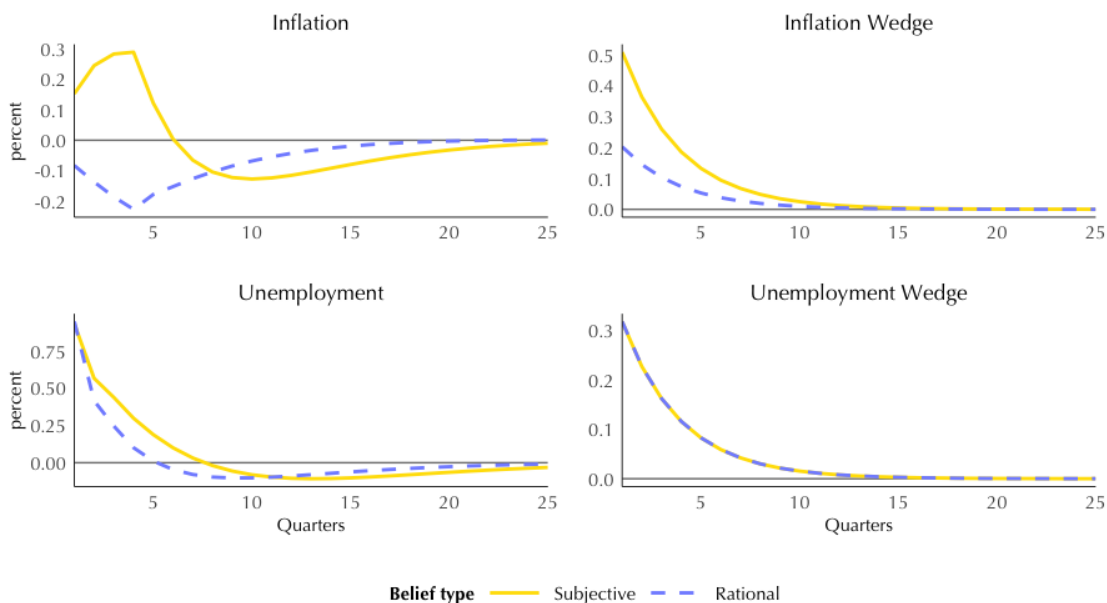
In this subsection, I revisit the empirical study by [Bhandari et al. \(2024\)](#), which explores the impact of subjective beliefs on macroeconomic aggregates. Their research develops a theory on how the bias of subjective beliefs from rational beliefs affects key economic indicators, formalizing these departures using model-consistent notions of pessimism and optimism.

The theoretical framework posits that fluctuations in beliefs, particularly increases in pessimism, have significant effects on the macroeconomy. This pessimism is hypothesized to be contractionary and to increase belief biases in both inflation and unemployment forecasts. The mechanism operates through various channels: pessimistic households lower current demand due to consumption smoothing, firms adjust their pricing and hiring strategies based on expectations of future economic conditions, and labor market

frictions amplify these effects. This shared pessimistic outlook creates a positive correlation between the biases in inflation and unemployment forecasts.

Figure 6 replicates the dynamic responses originally presented in Figure 10 of [Bhandari et al. \(2024\)](#). It compares the dynamic responses under two scenarios: one where all agents, including firms, hold subjective beliefs, and another where firms adopt rational expectations while households retain subjective beliefs. The solid line represents the case where all agents follow subjective beliefs, while the dashed line reflects the responses when firms adopt rational expectations. This comparison highlights important differences, where rational firms exhibit more muted fluctuations compared to the scenario where all agents are subjective. Specifically, rational firms keep inflation lower on impact, as they perceive an increase in pessimism as contractionary but do not anticipate higher future marginal costs, leading to smaller price adjustments. This figure provides a baseline understanding of the impulse responses under different belief structures, which will serve as the foundation for further analysis.

Figure 6: Impulse responses under subjective and rational beliefs



Notes. Replicated from Figure 10 in [Bhandari et al. \(2024\)](#). This figure compares impulse responses under two scenarios: subjective beliefs for all agents (solid line) and rational expectations for firms (dashed line).

To test this theory empirically, the authors utilize data from multiple sources. The key variable is the belief bias, which they term the “belief wedge”—defined as the difference

between subjective beliefs and rational forecasts. Subjective beliefs are measured using the University of Michigan Surveys of Consumers, while rational predictions are constructed using both VAR predictions and forecasts from the Survey of Professional Forecasters (SPF). The study focuses on quarterly data from 1982Q1 to 2019Q4.

Since their model predicts a one-factor structure of the belief wedges, they define the belief shock as the first principal component derived from the standardized inflation belief wedge and unemployment belief wedge. To address a possible misspecification of VAR forecasts and hence the belief wedges, the authors construct a belief shock using the principal component of the belief wedges between the Michigan and SPF forecasts. The question here is how positive deviation to this belief shock (pessimism) affects the economy.

The general estimating equation can be written as:

$$y_{t+h} = \beta_h \theta_t + \sum_{\ell=1}^L \delta_\ell \theta_{t-\ell} + \mathbf{w}'_t \gamma + u_{t,h}, \quad (5.2)$$

where θ_t is the belief shock, the first PC of the inflation and unemployment belief wedges, \mathbf{w}_t includes additional controls, and $u_{t,h}$ the error term.

Baseline Analysis and Robustness Across Specifications

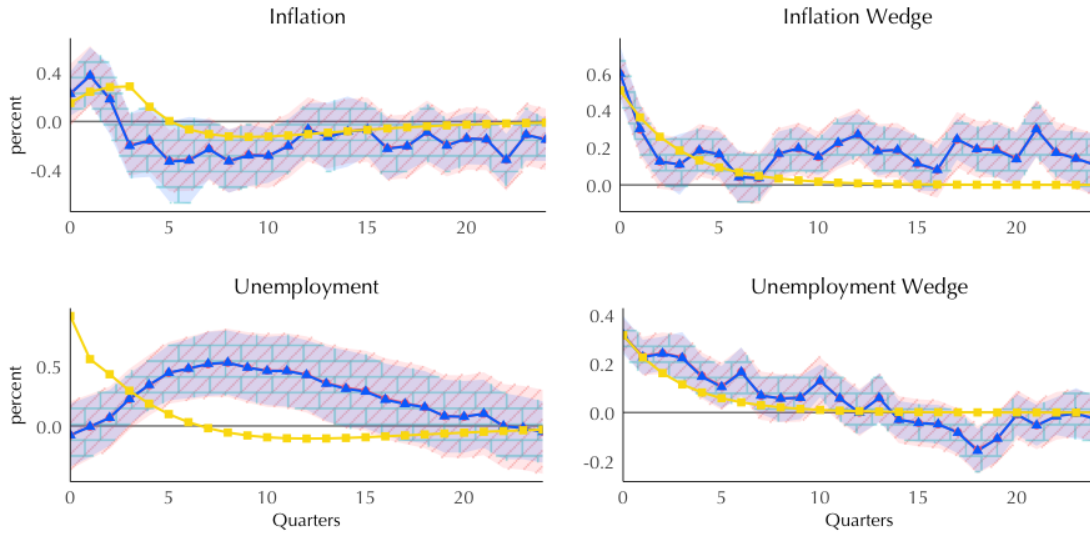
Figures 7–8 present the responses of the inflation, unemployment, and the belief wedges to a positive innovation in the belief shock across different model specifications. Each set of responses is estimated using the conventional LP and the proposed method. To provide context, the model-implied impulse response functions are included, where all agents are assumed to hold subjective beliefs. This provides a theoretical benchmark against which the empirical results can be evaluated.

I begin by presenting the results for the baseline model, where no additional controls are included and the lag order is set to 4. As shown in Figure 7a, the empirical results generally align with the model's predictions. Both LPs and the model show initial increases in inflation. While the model does not generate the hump-shaped responses by both methods, the authors say the magnitude is comparable to what the model implies. These outcomes align with increased pessimism, resulting in higher unemployment and inflation wedges. This alignment provides initial support for the robustness of the original study's conclusions.

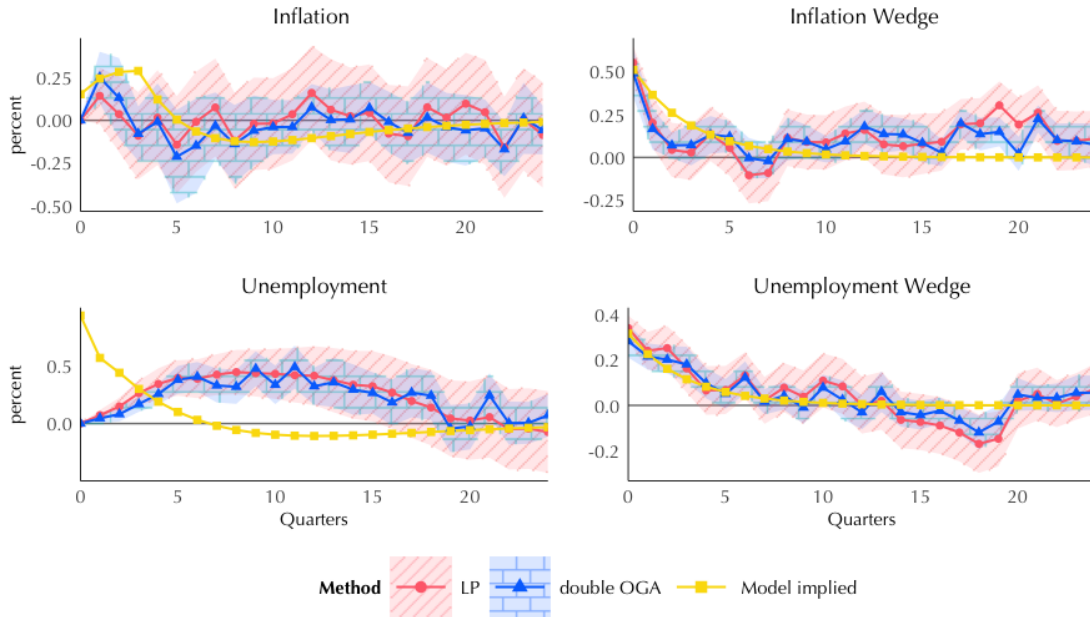
To ensure robustness, alternative model specifications are considered, including adding

Figure 7: Baseline and VAR controls added models with 4 lags

(a) Baseline with 4 lags



(b) VAR controls with 4 lags



Notes. This figure compares the baseline model with 4 lags (Panel (a)) and the VAR controls added model with 4 lags (Panel (b)) for inflation, inflation wedge, unemployment, and unemployment wedge. Point estimates are shown as solid lines with circle markers for LP (red), triangle markers for double OGA (blue), and square markers for model-implied (yellow). Shaded areas represent 90% confidence intervals, with diagonal shading for LP and brick-shaped shading for double OGA.

variables used to create the VAR forecasts as controls and increasing their lags. These controls, \mathbf{w}_t in (5.2), include key economic indicators such as GDP, inflation, unemployment, among others.

Invoking the recursive identification scheme, this approach assumes that these economic factors influence the belief shock variable, while the belief shock does not, in turn, affect these factors. This assumption aligns intuitively, as both subjective beliefs and rational forecasts are derived from the current state of economic indicators. The picture becomes more complex when additional controls are introduced. When I added the 9 variables used for the VAR prediction with 4 lags (Figure 7b), the standard errors for the conventional LP increased substantially. This increase in uncertainty makes it challenging to interpret some results coming from LP, particularly for inflation, where no significant effects are observed.

Further increasing the lags to 8 and 10 (Figures 8a and 8b), the conventional LP produces increasingly erratic results with inconsistent patterns. In contrast, the proposed method maintains consistent results with narrower confidence intervals across different specifications. Notably, the proposed method closely mimics the model-implied impulse responses, with the exception of unemployment. While neither methods do not comply with the model-implied responses for unemployment, the proposed method consistently find an approximately 0.5 percent increase in unemployment in magnitude across all model specifications.

These results reveal important insights about the robustness of different estimation methods across various model specifications. As the number of included variables and lags increases, the conventional LP method shows increasing variability in its results, producing wiggly estimates with wider standard errors. In contrast, the proposed method demonstrates remarkable robustness, maintaining consistent patterns and narrower confidence intervals across different specifications.

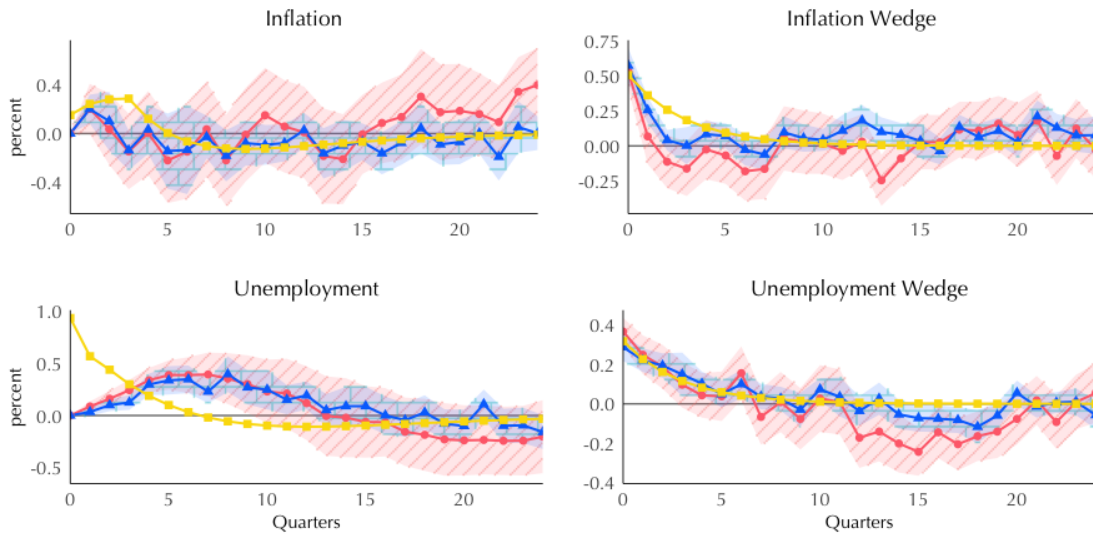
This robustness becomes particularly evident when the model includes more variables and higher lag orders. Importantly, the proposed method performs consistently in both simple and more complex settings, suggesting there's no disadvantage to using it when the underlying model structure is uncertain—a common scenario in empirical analysis.

For comparison, I also ran debiased LASSO⁴ from Adamek et al. (2024) in Figure 9. The results with other model specifications are in Appendix D.1, where debiased LASSO shows similar patterns across different model specifications. In particular, the method

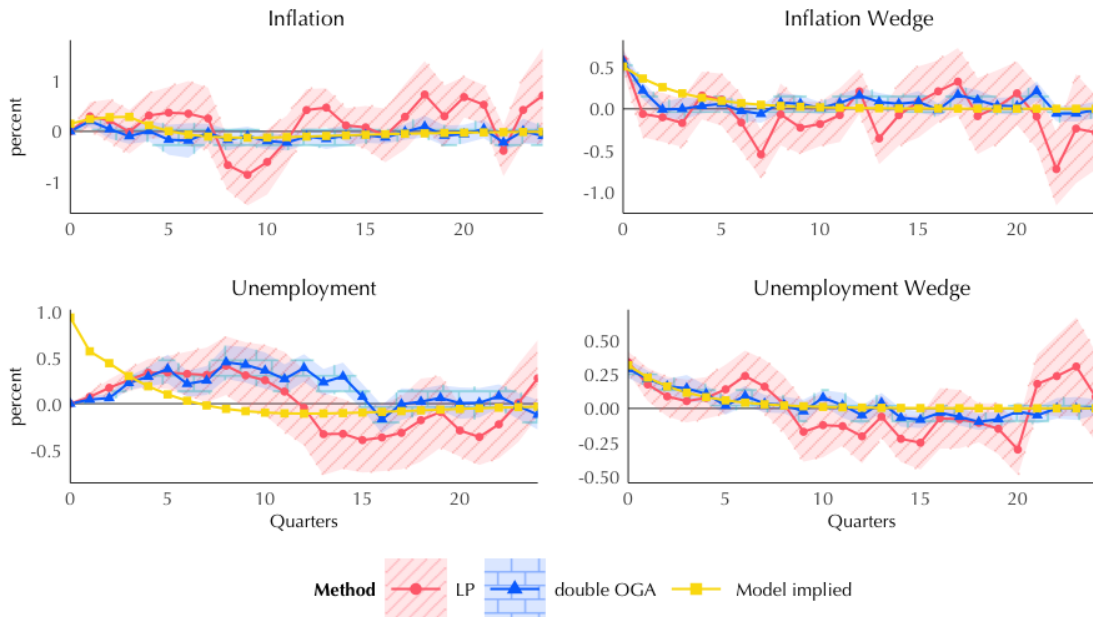
⁴For the debiased lasso estimation, I use the R package *desla* provided by Adamek et al. (2024).

Figure 8: VAR controls added models with longer lags

(a) VAR controls with 8 lags



(b) VAR controls with 10 lags



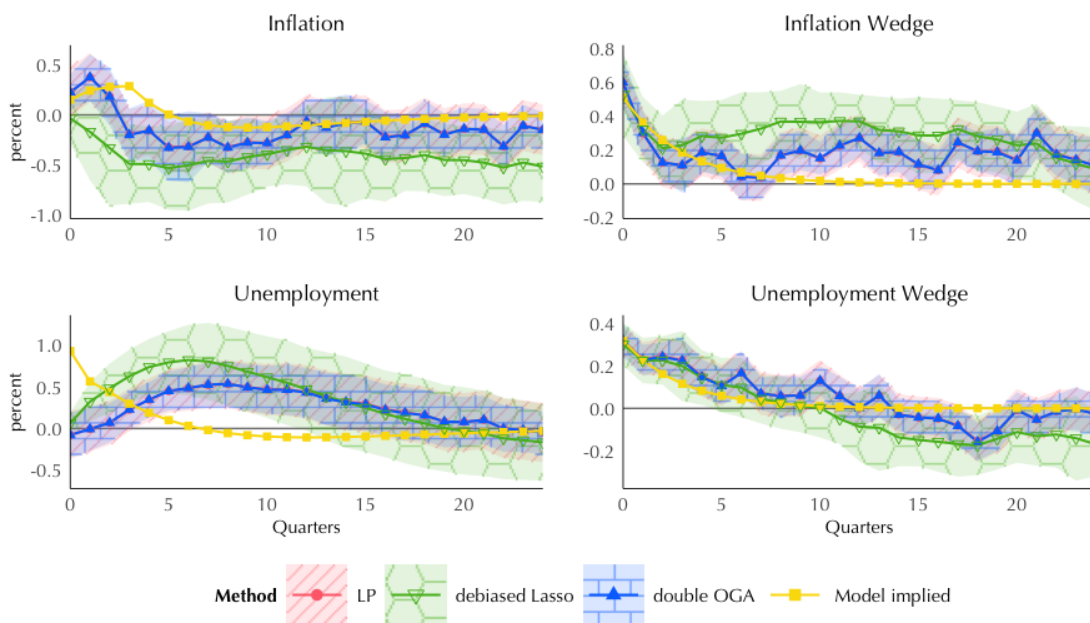
Method —●— LP —▲— double OGA —■— Model implied

Notes. This figure compares the VAR controls added model with 8 lags (Panel (a)) and with 10 lags (Panel (b)) for inflation, inflation wedge, unemployment, and unemployment wedge. Point estimates are shown as solid lines with circle markers for LP (red), triangle markers for double OGA (blue), and square markers for model-implied (yellow). Shaded areas represent 90% confidence intervals, with diagonal shading for LP and brick-shaped shading for double OGA.

yields highly persistent responses for inflation and inflation wedges. The unemployment response, while significant, tends to be overestimated, and the unemployment wedge exhibits a persistent negative bias over longer horizons.

These results are challenging to interpret both intuitively and within the theoretical perspective proposed by Bhandari et al. (2024). One possible explanation is that these models are relatively low-dimensional, which is not an ideal setting for LASSO. Alternatively, as suggested by the simulations, the high persistence in the data might be driving the estimates away from expected values.

Figure 9: Baseline model with debiased LASSO



Notes. This figure compares the baseline model for inflation, inflation wedge, unemployment, and unemployment wedge. Point estimates are shown as solid lines with circle markers for LP (red), inverted triangle markers for debiased LASSO (green), triangle markers for double OGA (blue), and square markers for model-implied (yellow). Shaded areas represent 90% confidence intervals, with diagonal shading for LP, hexagonal shading for debiased LASSO, and brick-shaped shading for double OGA.

State-Dependent Responses to Belief Shocks

Another findings of their paper is the cyclical patterns in the belief wedges. While their empirical analysis only included the baseline model for impulse responses, I extend the analysis by exploring different empirical specifications to account for the cyclicity. To

examine how the impulse responses differ across different economic conditions, I use NBER recession indicators to separate belief shocks into those occurring in bad states (θ_t^b) during recessions and good states (θ_t^g) outside of recession periods. If this specification shows no difference in responses, we can conclude that economic states do not significantly alter the effects of pessimism shocks. However, if we observe differences, we can infer important implications from these results. The model is specified as follows:

$$y_{t+h} = \beta_h^g \theta_t^g + \beta_h^b \theta_t^b + \sum_{\ell=1}^L \delta_\ell \theta_{t-\ell} + \mathbf{w}'_t \gamma + u_{t,h},$$

where the key interest lies in comparing the estimates of β_h^g and β_h^b . I begin with a baseline model without controls, then add controls used in VAR predictions, with both 4 and 8 lags in subsequent models.

In terms of results, I focus on inflation as it shows noticeable differences between good and bad states. The results for other dependent variables are presented in Appendix D.2, where they generally behave similarly across states: increase in both wedges, and hump-shaped patterns for the unemployment. However, inflation exhibits distinctive patterns depending on the economic state. Figure 10 shows the responses of inflation in good (left panel) and bad (right panel) states. For the baseline model, there is no clear pattern in good states, as no significant effects are observed. In bad states, we observe an initial positive response followed by negative responses. The behavior in bad states, especially for early horizons, resembles the subjective agent model predictions from Bhandari et al. (2024), as shown in Figure 6.

As in the previous discussion, adding controls make intuitive sense in that key economic indicators affect in the formation of both the subjective and rational beliefs. Importantly, focusing on the models with VAR controls, the proposed model yields robust estimates regardless of lag length. And this is where we see more obvious patterns. Unlike in the baseline model where we couldn't find any significant effect for the good state, we now see significant negative responses in the beginning horizons, in both models regardless of the lag length. Also, we observe significant positive responses in bad states, while the magnitude is smaller than what the model predicts. For convenience, I also included the point estimates and the standard errors in Table 1. For the bad states in subtable (b), we do see positive point estimates compared to negative ones in the good states counterparts.

These findings suggest that the economy behaves more rationally in good states, even in the presence of a pessimism shock, while firms act more like subjective agents in bad states.

In good states, as in the rational firms model of [Bhandari et al. \(2024\)](#), firms recognize a pessimism shock but do not associate it with higher future inflation, leading to only a slight and temporary dip in inflation before recovery. This behavior reflects a confidence in the economy's strong fundamentals, which prevents firms from overreacting to the shock.

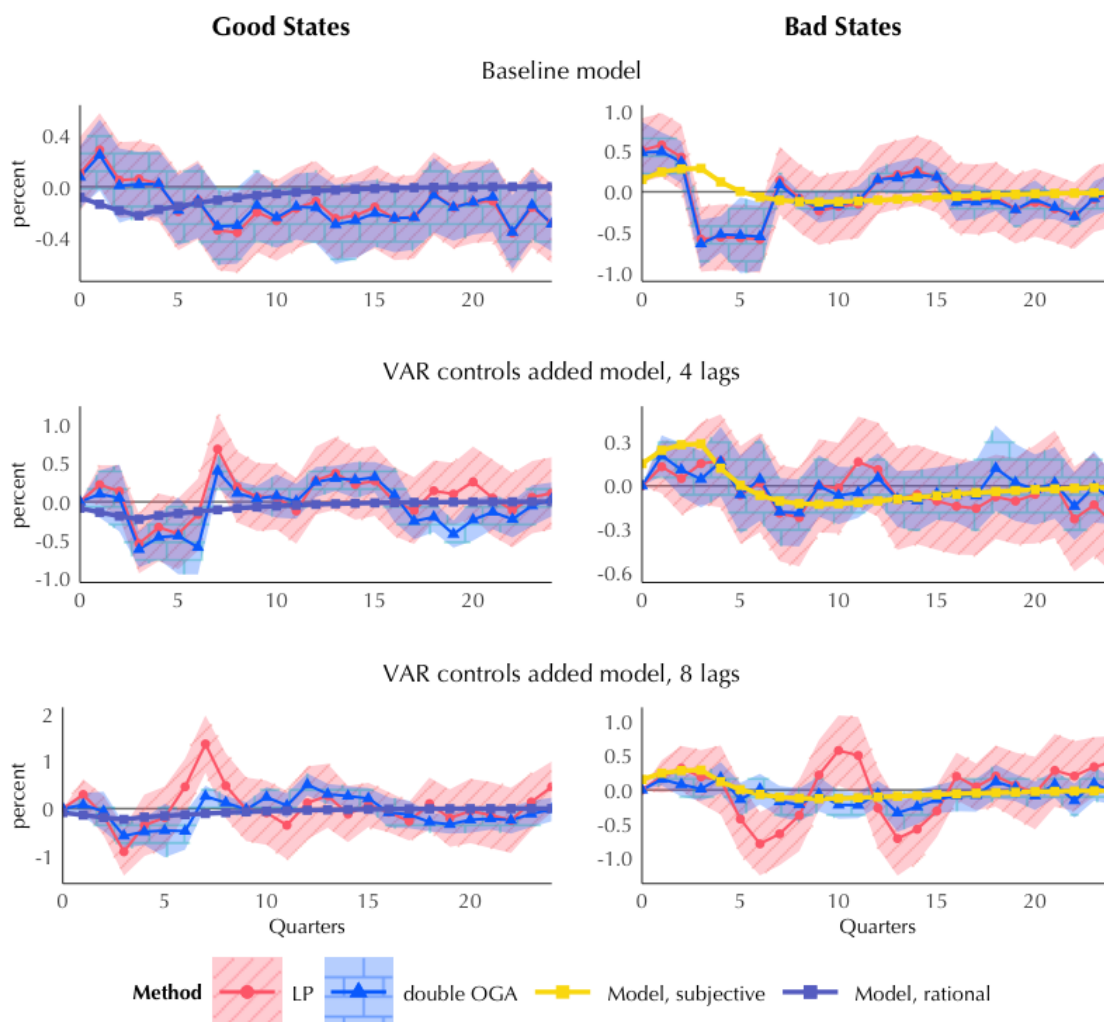
In bad states, however, pessimism raises the subjective probability of negative outcomes like lower productivity and tighter monetary policy, as noted by the subjective agents model of [Bhandari et al. \(2024\)](#). This leads firms to expect higher future marginal costs, thus reducing their incentive to lower prices even during a contraction. The “muted” inflation response in bad states, which actually involves an increase in inflation, is due to firms' defensive pricing behavior as they brace for worsening conditions. This mirrors [Shiller \(2003\)](#)'s concept of negative feedback loops where bad economic states reinforce pessimism, leading to irrational decisions and inflationary pressures as firms anticipate continued declines in productivity and demand.

In summary, the empirical analysis largely supports the findings of [Bhandari et al. \(2024\)](#), showing that positive shocks to belief wedges lead to increases in both inflation and unemployment, consistent with the hypothesized effects of heightened pessimism. The proposed method demonstrates robustness across different model specifications, producing stable results with added controls and varying lag lengths. A key contribution of this analysis is the exploration of belief shock responses in different economic states. In good states, inflation shows a temporary dip followed by recovery, reflecting rational firm behavior. However, in bad states, inflation increases, driven by firms' pessimistic expectations of higher future marginal costs, as predicted by the subjective agent model. This state-dependent inflation response highlights the role of economic conditions in shaping the effects of pessimism shocks. While other variables, such as unemployment, exhibit consistent dynamics across states, the differentiated inflation response underscores the importance of considering state-dependent behaviors in empirical analyses. These results open avenues for future research to refine theoretical models to account for these distinct patterns across economic conditions.

6 Concluding Remarks

Local projection has emerged as the preferred alternative to VARs in impulse response analysis due to its robustness to model misspecification and ease of implementation ([Mon-tiel Olea and Plagborg-Møller, 2021](#); [Olea, Plagborg-Møller, Qian, and Wolf, 2024](#)). As the

Figure 10: Impulse responses of inflation with good and bad states



Notes. This figure illustrates the impulse responses of inflation to a belief shock in both good and bad states under various model specifications. The good states (left panels) and bad states (right panels) are identified by NBER recession indicators. The model specifications include a baseline model and models with added VAR controls (4 lags and 8 lags).

use of local projections has gained traction, recent literature has addressed the challenges of incorporating high-dimensional covariates, with a particular focus on methods like LASSO. However, the reliance on strong sparsity assumptions in these methods limits their applicability in many empirical settings, especially when dense DGPs are present.

This paper aims to address the gap in the literature by introducing a high-dimensional local projection approach that caters to both sparse and dense settings and takes into

account the uncertainty of sparseness in the DGP. Building on the OGA with HDAIC method proposed by Ing (2020), the proposed method relaxes the need for strict sparsity by allowing parameters to decay toward zero as dimensionality increases, making it especially suitable for economic time series with autoregressive properties.

The proposed framework demonstrates significant advantages in both DiD estimation and impulse response analysis. In addition, the proposed approach has the advantage of interpretability through the use of OGA, which orders covariates based on their explanatory power. Through simulations, I show strong performance in handling persistent data and longer horizons estimations.

By utilizing the OGA with HDAIC and the NED assumptions, the local projection estimator achieves \sqrt{T} asymptotic normality with HAC standard errors. The theoretical foundation of this method is based on the error bounds of Ing (2020), the triplex inequality of Jiang (2009), and double selection arguments of Belloni et al. (2013). These advances strengthen the framework's capacity to handle complex time series data while maintaining reliable inference.

In conclusion, this method advances econometric modeling by offering a practical, robust solution for high-dimensional datasets. Its applicability to both sparse and dense scenarios makes it a practical tool for researchers working on a range of empirical applications, from macroeconomic analysis to event studies, providing a framework that ensures consistency and reliability across a broad range of empirical applications.

References

- ABADIE, A. (2005): "Semiparametric difference-in-differences estimators," *The review of economic studies*, 72, 1–19.
- ACEMOGLU, D., S. NAIDU, P. RESTREPO, AND J. A. ROBINSON (2019): "Democracy does cause growth," *Journal of Political Economy*, 127, 47–100.
- ADAMEK, R., S. SMEEKES, AND I. WILMS (2023): "Lasso inference for high-dimensional time series," *Journal of Econometrics*, 235, 1114–1143.
- (2024): "Local projection inference in high dimensions," *The Econometrics Journal*, utae012.
- ANDREWS, D. W. (1991): "Heteroskedasticity and autocorrelation consistent covariance matrix estimation," *Econometrica*, 817–858.
- ANGRIST, J. D., Ò. JORDÀ, AND G. M. KUERSTEINER (2018): "Semiparametric Estimates of Monetary Policy Effects: String Theory Revisited," *Journal of Business & Economic Statistics*, 36, 371–387.
- BELLONI, A., V. CHERNOZHUKOV, AND C. HANSEN (2013): "Inference on Treatment Effects after Selection among High-Dimensional Controlst," *Review of Economic Studies*, 81, 608–650.
- BHANDARI, A., J. BOROVÍČKA, AND P. HO (2024): "Survey data and subjective beliefs in business cycle models," *Review of Economic Studies*, rdae054.
- BICKEL, P. J., Y. RITOV, AND A. B. TSYBAKOV (2009): "Simultaneous analysis of Lasso and Dantzig selector," *The Annals of Statistics*, 37, 1705–1732.
- CALLAWAY, B. AND P. H. SANT'ANNA (2021): "Difference-in-differences with multiple time periods," *Journal of econometrics*, 225, 200–230.
- CHA, J., H. D. CHIANG, AND Y. SASAKI (2023): "Inference in High-Dimensional Regression Models without the Exact or L_p Sparsity," *Review of Economics and Statistics*, 1–32.
- CHERNOZHUKOV, V., W. K. HÄRDLE, C. HUANG, AND W. WANG (2021): "LASSO-driven inference in time and space," *The Annals of Statistics*, 49, 1702 – 1735.

- DAVIDSON, J. (1994): *Stochastic limit theory: An introduction for econometricians*, Oxford University Press.
- (2021): *Stochastic limit theory: An introduction for econometricians (2nd ed.)*, Oxford University Press.
- DINH, V. H., D. NIBBERING, AND B. WONG (2024): “Random Subspace Local Projections,” *arXiv preprint arXiv:2406.01002*.
- DUBE, A., D. GIRARDI, O. JORDA, AND A. M. TAYLOR (2023): “A local projections approach to difference-in-differences event studies,” Tech. rep., National Bureau of Economic Research.
- D’AMOUR, A., P. DING, A. FELLER, L. LEI, AND J. SEKHON (2021): “Overlap in observational studies with high-dimensional covariates,” *Journal of Econometrics*, 221, 644–654.
- GIANNONE, D., M. LENZA, AND G. E. PRIMICERI (2021): “Economic predictions with big data: The illusion of sparsity,” *Econometrica*, 89, 2409–2437.
- HANSEN, B. E. (1991): “Strong laws for dependent heterogeneous processes,” *Econometric theory*, 7, 213–221.
- HECKMAN, J. J., H. ICHIMURA, J. A. SMITH, AND P. E. TODD (1998): “Characterizing selection bias using experimental data,” .
- HECKMAN, J. J., H. ICHIMURA, AND P. E. TODD (1997): “Matching as an econometric evaluation estimator: Evidence from evaluating a job training programme,” *The review of economic studies*, 64, 605–654.
- ING, C.-K. (2020): “Model selection for high-dimensional linear regression with dependent observations,” *The Annals of Statistics*, 48, 1959–1980.
- JIANG, W. (2009): “On Uniform Deviations of General Empirical Risks with Unbound- edness, Dependence, and High Dimensionality.” *Journal of Machine Learning Research*, 10.
- JORDÀ, Ò. (2005): “Estimation and inference of impulse responses by local projections,” *American Economic Review*, 95, 161–182.

- KÄNZIG, D. R. (2021): “The macroeconomic effects of oil supply news: Evidence from OPEC announcements,” *American Economic Review*, 111, 1092–1125.
- KOLESÁR, M., U. K. MÜLLER, AND S. T. ROELSGAARD (2023): “The Fragility of Sparsity,” *arXiv preprint arXiv:2311.02299*.
- MONTIEL OLEA, J. L. AND M. PLAGBORG-MØLLER (2021): “Local Projection Inference Is Simpler and More Robust Than You Think,” *Econometrica*, 89, 1789–1823.
- OLEA, J. L. M., M. PLAGBORG-MØLLER, E. QIAN, AND C. K. WOLF (2024): “Double Robustness of Local Projections and Some Unpleasant VARithmetic,” Tech. rep., National Bureau of Economic Research.
- PLAGBORG-MØLLER, M. AND C. K. WOLF (2021): “Local projections and VARs estimate the same impulse responses,” *Econometrica*, 89, 955–980.
- ROSENBAUM, P. R. AND P. R. ROSENBAUM (2002): *Overt bias in observational studies*, Springer.
- RUBIN, D. B. (1974): “Estimating causal effects of treatments in randomized and nonrandomized studies.” *Journal of Educational Psychology*, 66, 688.
- SEMENOVA, V., M. GOLDMAN, V. CHERNOZHUKOV, AND M. TADDY (2023): “Inference on heterogeneous treatment effects in high-dimensional dynamic panels under weak dependence,” *Quantitative Economics*, 14, 471–510.
- SHILLER, R. J. (2003): “From efficient markets theory to behavioral finance,” *Journal of economic perspectives*, 17, 83–104.
- STOCK, J. AND M. WATSON (2016): “Chapter 8 - Dynamic Factor Models, Factor-Augmented Vector Autoregressions, and Structural Vector Autoregressions in Macroeconomics,” Elsevier, vol. 2 of *Handbook of Macroeconomics*, 415–525.
- STOCK, J. H. AND M. W. WATSON (2002): “Forecasting using principal components from a large number of predictors,” *Journal of the American Statistical Association*, 97, 1167–1179.
- VAN DE GEER, S., P. BÜHLMANN, Y. RITOV, AND R. DEZEURE (2014): “On asymptotically optimal confidence regions and tests for high-dimensional models,” *The Annals of Statistics*, 42, 1166–1202.

WANG, Z., S. PATERLINI, F. GAO, AND Y. YANG (2014): “Adaptive minimax regression estimation over sparse l_q -hulls,” *The Journal of Machine Learning Research*, 15, 1675–1711.

ZHANG, C.-H. AND S. S. ZHANG (2014): “Confidence intervals for low dimensional parameters in high dimensional linear models,” *Journal of the Royal Statistical Society Series B: Statistical Methodology*, 76, 217–242.

A Proof of Main Theorems

Notations. For a vector $X = (X_1, \dots, X_p)'$, $\|X\|_q = (\sum_{j=1}^p X_j^q)^{1/q}$ denotes the L- q norm for $q < \infty$ and $\|X\|_\infty = \max_{1 \leq j \leq p} |X_j|$.

A.1 Proof of Theorem 4.1

Proof. The main purpose of this proof is to show that the assumptions (2.33) and (2.34) in Ing (2020) hold under Assumptions 1 – 4. Since the estimating equations are (2.3) and (2.4), the assumptions should hold on the two equations.

I start with condition (2.34) in Ing (2020) because it is a stringent condition than (2.33). It states that there exists a constant $c > 0$ such that

$$P \left(\max_{1 \leq j, k \leq p, j \neq k} \left| \frac{1}{T} \sum_{t=1}^T w_{t,j} w_{t,k} - E[w_{t,j} w_{t,k}] \right| \geq c \sqrt{\frac{(\log p)^3}{T}} \right) = o(1). \quad (\text{A.1})$$

For any $x \geq 0$, it follows from the union bound that

$$\begin{aligned} P \left(\max_{1 \leq j, k \leq p, j \neq k} \left| \frac{1}{T} \sum_{t=1}^T w_{t,j} w_{t,k} - E[w_{t,j} w_{t,k}] \right| \geq x \right) \\ \leq \sum_{j=1}^p \sum_{k=1}^p P \left(\left| \frac{1}{T} \sum_{t=1}^T w_{t,j} w_{t,k} - E[w_{t,j} w_{t,k}] \right| \geq x \right) \\ \leq p^2 P \left(\left| \frac{1}{T} \sum_{t=1}^T w_{t,j} w_{t,k} - E[w_{t,j} w_{t,k}] \right| \geq x \right). \end{aligned}$$

Notice that by Lemma 4.3 (c), we can apply the triplex inequality Lemma 4.2,

$$\begin{aligned} p^2 P \left(\left| \frac{1}{T} \sum_{t=1}^T w_{t,j} w_{t,k} - E[w_{t,j} w_{t,k}] \right| \geq x \right) \\ \leq 2p^2 m \exp \left(-\frac{Tx^2}{288m^2 M^2} \right) \end{aligned} \quad (\text{BD1})$$

$$+ \frac{6\bar{c}_T}{x} p^2 \rho_m \quad (\text{BD2})$$

$$+ \frac{15C}{x} p^2 \exp(-M(\bar{q} - 1)), \quad (\text{BD3})$$

where m is a positive integer number and $M > 0$ is some constant. I proceed by showing

that there is a sequence $\eta_T \rightarrow 0$ as $T \rightarrow \infty$ that bounds all the components (BD1) – (BD3). Since Lemma 4.2 holds for all positive integer m and a constant $M > 0$, the bounds can be further simplified by defining m and M in terms of T and p (Jiang (2009), Remark 2). Let $M = c_M \log p$ and $m = 1$, where $c_M > 2/(\bar{q} - 1)$. To match the convergence rate in (A.1), let $x = c_1((\log p)^3/T)^{1/2}$, where $c_1 > 24c_M$. By Assumption 2, $\rho_m \leq \exp(-c_\kappa \log p)$, and the bounds become

$$\begin{aligned} & P \left(\max_{1 \leq j, k \leq p, j \neq k} \left| \frac{1}{T} \sum_{t=1}^T w_{t,j} w_{t,k} - E[w_{t,j} w_{t,k}] \right| \geq x \right) \\ & \leq Cp^2 \exp \left(-\frac{c_1^2}{288c_M^2} \log p \right) \\ & \quad + Cx^{-1} p^2 \exp(-c_\kappa \log p) \\ & \quad + Cx^{-1} p^2 \exp(-c_M(\bar{q} - 1) \log p), \end{aligned}$$

where I abuse the notation C for a generic constant, because only the constants inside the exponential terms matter. The first term is $o(1)$ if $c_1^2/(288c_M^2) > 2$, which is satisfied by setting $c_1 > 24c_M$. Similarly, the second and the third term are $o(1)$ if $c_\kappa > 2$ and $c_M(\bar{q} - 1) > 2$, which is satisfied by definitions of the constants. Therefore, all terms are $o(1)$ and hence equation A.1 is satisfied.

Next we turn to condition (2.32) in Ing (2020). It states that there exists a constant $c > 0$ such that

$$P \left(\max_{1 \leq j \leq p} \left| \frac{1}{T} \sum_{t=1}^T w_{t,j} e_{t,h} \right| \geq c \sqrt{\frac{(\log p)^3}{T}} \right) = o(1) \quad (\text{A.2})$$

and

$$P \left(\max_{1 \leq j \leq p} \left| \frac{1}{T} \sum_{t=1}^T w_{t,j} v_{t,h} \right| \geq c \sqrt{\frac{(\log p)^3}{T}} \right) = o(1), \quad (\text{A.3})$$

for all $h = 1, \dots, H_{\max}$.

Consider the case with $\{w_{t,j} e_{t,h}\}$. Applying the union bound, for any $x \geq 0$ it holds that

$$P \left(\max_{1 \leq j \leq p} \left| \frac{1}{T} \sum_{t=1}^T w_{t,j} e_{t,h} - E[w_{t,j} e_{t,h}] \right| \geq x \right)$$

$$\begin{aligned}
&\leq \sum_{j=1}^p P \left(\left| \frac{1}{T} \sum_{t=1}^T w_{t,j} e_{t,h} - E[w_{t,j} e_{t,h}] \right| \geq x \right) \\
&\leq p P \left(\left| \frac{1}{T} \sum_{t=1}^T w_{t,j} e_{t,h} - E[w_{t,j} e_{t,h}] \right| \geq x \right).
\end{aligned}$$

By Assumption 2.2 and Lemma 4.3 (b), we can apply Lemma 4.2, and

$$\begin{aligned}
&p P \left(\left| \frac{1}{T} \sum_{t=1}^T w_{t,j} e_{t,h} - E[w_{t,j} e_{t,h}] \right| \geq x \right) \\
&\leq Cp \exp \left(-\frac{c_1^2}{288c_M^2} \log p \right) \\
&\quad + Cx^{-1} p \exp(-c_\kappa \log p) \\
&\quad + Cx^{-1} p \exp(-c_M(\bar{q} - 1) \log p),
\end{aligned}$$

where all three terms are bounded by $\eta_T \rightarrow 0$ used to bound (BD1) – (BD3) since the above right hand side terms grow at a slower rate, by p^{-1} . Therefore, (A.2) holds.

The same argument applies for $\{w_{t,j} v_{t,h}\}$ case, because Assumption 2.2 and Lemma 4.3 applies analogously with same constants $\{c_t\}$ and ρ_m . By Lemma 4.2, all three terms are bounded by the same $\eta_T \rightarrow 0$, and hence (A.3) holds.

Assumptions (A3) in Ing (2020) are assumed in Assumption 3 and Assumption (A5) in Ing (2020) is assumed in Assumption 4 (a). This set of assumptions collectively satisfies the necessary conditions outlined in Theorem 3.1 of Ing (2020), thereby yielding the desired results. \square

A.2 Proof of Theorem 4.2

Proof. In this proof, I use notations in (4.9). Further, write (4.9) as

$$\begin{aligned}
\mathbf{y}_h &= \beta_h \mathbf{x}_h + W_h \beta_{-h} + \mathbf{u}_h =: \beta_h \mathbf{x}_h + \mathbf{g} + \mathbf{u}_h, \\
\mathbf{x}_h &= W_h \gamma_h + \mathbf{v}_h =: \mathbf{m} + \mathbf{v}_h,
\end{aligned} \tag{A.4}$$

where \mathbf{g} and \mathbf{m} are functions of W_h . In the following proof, I first show the probability limit of $\sqrt{T}(\hat{\beta}_h - \beta)$ using similar arguments in Belloni et al. (2013) and then derive asymptotic distribution of it using Theorem 25.12 in Davidson (2021).

Recall the subset of the covariates notation $W_h(J) = (W_{h,j})_{j \in J}$ and denote $\hat{\Sigma}(J) =$

$W_h(J)'W_h(J)/T$. Define

$$\begin{aligned}\sqrt{T}(\widehat{\beta}_h - \beta) &= (\mathbf{x}'_h M \mathbf{x}_h / T)^{-1} (\mathbf{x}'_h M (\mathbf{g} + \mathbf{u}_h) / \sqrt{T}) \\ &=: A^{-1} B,\end{aligned}$$

where $M_J := I - P_J$ and $P_J = W_h(J)(W_h(J)'W_h(J))^{-1}W_h(J)'$. Define $\widetilde{J} = \widehat{J}_x \cup \widehat{J}_y$, where \widehat{J}_x and \widehat{J}_y are the chosen covariates from the steps 1 and 2 in Algorithm 1. Also, let $\widetilde{\gamma}_h$ the projection coefficient of \mathbf{x}_h onto span $W_h(\widetilde{J})$ and let $\widetilde{\alpha}_h$ be the projection coefficient of \mathbf{v}_h onto span $W_h(\widetilde{J})$, respectively.

I will proceed by showing that

$$A = \mathbf{v}'_h \mathbf{v}_h / T + o_p(1), \quad B = \mathbf{v}'_h \mathbf{u}_h / \sqrt{T} + o_p(1).$$

Decompose A and B into pieces using (A.4).

$$\begin{aligned}A &= (\mathbf{x}'_h M_{\widetilde{J}} \mathbf{x}_h) / T \\ &= (\mathbf{m} + \mathbf{v}_h)' M_{\widetilde{J}} (\mathbf{m} + \mathbf{v}_h) / T \\ &= \mathbf{m}' M_{\widetilde{J}} \mathbf{m} / T + 2\mathbf{m}' M_{\widetilde{J}} \mathbf{v}_h / T + \mathbf{v}'_h \mathbf{v}_h / T - \mathbf{v}'_h P_{\widetilde{J}} \mathbf{v}_h / T, \\ B &= \mathbf{x}'_h M_{\widetilde{J}} (\mathbf{g} + \mathbf{u}_h) / \sqrt{T} \\ &= (\mathbf{m} + \mathbf{v}_h)' M_{\widetilde{J}} (\mathbf{g} + \mathbf{u}_h) / \sqrt{T} \\ &= \mathbf{m}' M_{\widetilde{J}} \mathbf{g} / \sqrt{T} + \mathbf{m}' M_{\widetilde{J}} \mathbf{u}_h / \sqrt{T} + \mathbf{v}'_h M_{\widetilde{J}} \mathbf{g} / \sqrt{T} + \mathbf{v}'_h \mathbf{u}_h / \sqrt{T} - \mathbf{v}'_h P_{\widetilde{J}} \mathbf{u}_h / \sqrt{T}.\end{aligned}$$

Notice that the pieces in A and B can be bounded similarly, except the bounds in B should be more restrictive. Each piece in A and B can be then decomposed into components, using idempotent property of the orthogonal projection matrix M . Below are the components used as ingredients for bounding A and B .

i) Bounds for $\|W'_h \mathbf{v}_h / T\|_\infty$ and $\|W'_h \mathbf{u}_h / T\|_\infty$

From the proof of Theorem 4.1, (A.2) and (A.3) holds, and hence

$$\|W'_h \mathbf{v}_h / T\|_\infty = O_p \left(\left((\log p)^3 / T \right)^{1/2} \right), \quad (\text{A.5})$$

and the same argument applies to $\|W'_h \mathbf{u}_h / T\|_\infty$ because $e_{t,h}$ and $u_{t,h}$ share the same assumption in Assumption 1.

ii) Bounds for $\|\tilde{\gamma}_h - \gamma_h\|$ and $\|\hat{\beta}_{-h} - \beta_{-h}\|$

Recall from Assumption 4 (b) and Theorem 4.1 we have

$$\begin{aligned}\|\hat{\gamma}_h - \gamma_h\| &\leq \left(\Lambda_{\min}^{-1} E_T \left[\frac{1}{T} \sum_{t=1}^T ((\hat{\gamma}_h - \gamma_h)' \mathbf{w}_t)^2 \right] \right)^{1/2} \\ &= O_p \left(\left(\frac{(\log p)^3}{T} \right)^{(2\delta-1)/(4\delta)} \right).\end{aligned}$$

Similarly,

$$\begin{aligned}\|\hat{\beta}_{-h} - \beta_{-h}\| &\leq \left(\Lambda_{\min}^{-1} E_T \left[\frac{1}{T} \sum_{t=1}^T ((\hat{\beta}_{-h} - \beta_{-h})' \mathbf{w}_t)^2 \right] \right)^{1/2} \\ &\leq \left(\Lambda_{\min}^{-1} E_T \left[\frac{1}{T} \sum_{t=1}^T ((\hat{\lambda}_h - \lambda_h)' \mathbf{w}_t)^2 \right] \right) \\ &= O_p \left(\left(\frac{(\log p)^3}{T} \right)^{(2\delta-1)/(4\delta)} \right),\end{aligned}$$

where the first inequality comes from Assumption 4 (b), the second from $\tilde{J} \subset \hat{J}_y$, and the third from Theorem 4.1.

iii) Bounds for $\|M_{\tilde{J}}\mathbf{m}/\sqrt{T}\|$ and $\|M_{\tilde{J}}\mathbf{g}/\sqrt{T}\|$

It follows from the definition of $M_{\tilde{J}}$ and $\tilde{\gamma}_h$ that $M_{\tilde{J}}\mathbf{m} = (I - P_{\tilde{J}})W_h\gamma_h = W_h(\gamma_h - \tilde{\gamma}_h)$ and hence

$$\begin{aligned}\|M_{\tilde{J}}\mathbf{m}/\sqrt{T}\| &\leq \|W_h(\tilde{\gamma}_h - \gamma_h)/\sqrt{T}\| \\ &= O_p \left(\left(\frac{(\log p)^3}{T} \right)^{(2\delta-1)/(4\delta)} \right)\end{aligned}\tag{A.6}$$

from Theorem 4.1. For $\|M_{\tilde{J}}\mathbf{g}/\sqrt{T}\|$, it holds by equation (A.4) and triangle inequality that

$$\begin{aligned}\|M_{\tilde{J}_y}\mathbf{y}_h/\sqrt{T}\| &\geq \|M_{\tilde{J}}(\beta_h\mathbf{x}_h + \mathbf{g})/\sqrt{T}\| \\ &\geq \|\beta_h\| \left\| M_{\tilde{J}}\mathbf{x}_h/\sqrt{T} \right\| - \|M_{\tilde{J}}\mathbf{g}/\sqrt{T}\|,\end{aligned}$$

where $\|\beta_h\| \leq C$ by Assumption 3. Since $\|M_{\hat{J}_y} \mathbf{y}_h / \sqrt{T}\|$ and $\|M_{\tilde{J}} \mathbf{x}_h / \sqrt{T}\|$ share the same error bound by Theorem 4.1,

$$\|M_{\tilde{J}} \mathbf{g} / \sqrt{T}\| = O_p \left(\left(\frac{(\log p)^3}{T} \right)^{(2\delta-1)/(4\delta)} \right).$$

iv) Bounds for $\|\tilde{\gamma}_h - \gamma_h\|_1$ and $\|\hat{\beta}_{-h} - \beta_{-h}\|_1$

Denote $\gamma_h(J) = (\gamma_{j,h})_{j=1}^p$, where $\gamma_{k,h} = 0$ for all $k \notin J$. By triangle inequality it follows that

$$\begin{aligned} \|\tilde{\gamma}_h - \gamma_h\|_1 &\leq \|\tilde{\gamma}_h - \gamma_h(\tilde{J})\|_1 + \|\gamma_h(\tilde{J}^c)\| \\ &\leq \|\tilde{\gamma}_h - \gamma_h(\tilde{J})\|_1 + \|\gamma_h - \gamma_h(\tilde{J})\|_1. \end{aligned}$$

The first term is bounded by

$$\begin{aligned} \|\tilde{\gamma}_h - \gamma_h(\tilde{J})\|_1 &\leq \sqrt{|\tilde{J}|} \|\tilde{\gamma}_h - \gamma_h(\tilde{J})\| \\ &\leq \sqrt{\hat{m}^y + \hat{m}^x} \|\hat{\gamma}_h - \gamma_h(\hat{J}_x)\| \\ &\leq C \sqrt{M_T^*} \|\hat{\gamma}_h - \gamma_h(\hat{J}_x)\| \\ &= O_p \left(\left(\frac{(\log p)^3}{T} \right)^{(\delta-1)/(2\delta)} \right), \end{aligned}$$

where the second inequality comes from $\tilde{J} = \hat{J}^{[1]} \cup \hat{J}^{[2]}$ and the third from $P(\hat{m} \geq CM_T^*) = 0$, as proved in Section S2 of the Supplementary Material of Ing (2020). The fourth comes from the definition of M_T^* in equation (C.1) and the error bounds in Theorem 4.1. The second term can be bounded by

$$\begin{aligned} \|\gamma_h - \gamma_h(\tilde{J})\|_1 &\leq C \sum_{j \notin \tilde{J}} |\gamma_{j,h}| \\ &\leq CC_\delta \left(\sum_{j \notin \tilde{J}} \gamma_{j,h}^2 \right)^{(\delta-1)/(2\delta-1)} \\ &\leq CC_\delta \Lambda_{\min}^{(-\delta+1)/(2\delta-1)} \left(E_T \left[\frac{1}{T} \sum_{t=1}^T (\mathbf{x}_t - \tilde{\gamma}_h' \mathbf{w}_t)^2 \right] \right)^{(\delta-1)/(2\delta-1)} \end{aligned}$$

$$= O_p \left(\left(\frac{(\log p)^3}{T} \right)^{(\delta-1)/(2\delta)} \right),$$

where the first inequality comes from Assumption 4 (a): for all $J \subseteq \mathfrak{A}$ such that $|J| \leq C(T/(\log p)^3)^{1/2}$, the first inequality holds as shown in Ing (2020) equation (2.16) and the following equation. The second inequality follows from Assumption 3, the third is implied by Assumption 4 (b) and the error bounds from Theorem 4.1. Combining the two bounds, we have

$$\begin{aligned} \|\tilde{\gamma}_h - \gamma_h\|_1 &\leq \|\tilde{\gamma}_h - \gamma_h(\tilde{J})\|_1 + \|\gamma_h - \gamma_h(\tilde{J})\|_1 \\ &= O_p \left(\left(\frac{(\log p)^3}{T} \right)^{(\delta-1)/(2\delta)} \right). \end{aligned} \quad (\text{A.7})$$

Similar argument applies to $\|\hat{\beta}_{-h} - \beta_{-h}\|_1$, where $\|\hat{\beta}_{-h} - \beta_{-h}\|_1 \leq \|\hat{\beta}_{-h} - \beta_h(\tilde{J})\|_1 + \|\beta_h - \beta_h(\tilde{J})\|_1$ by triangle inequality. The two terms are bounded by

$$\begin{aligned} \|\hat{\beta}_h - \beta_h(\tilde{J})\|_1 &\leq \sqrt{|\tilde{J}|} \|\hat{\beta}_h - \beta_h(\tilde{J})\| \\ &\leq \sqrt{M_T^*} \|\hat{\lambda}_h - \lambda_h(\hat{J}_y)\| \\ &= O_p \left(\left(\frac{(\log p)^3}{T} \right)^{(\delta-1)/(2\delta)} \right) \end{aligned}$$

and

$$\begin{aligned} \|\beta_h(\hat{J}) - \beta_h\|_1 &\leq C \sum_{j \notin \hat{J}} |\beta_{j,-h}| \\ &\leq CC_\delta \left(\sum_{j \notin \hat{J}} \beta_{j,-h}^2 \right)^{(\delta-1)/(2\delta-1)} \\ &\leq CC_\delta \Lambda_{\min}^{(-\delta+1)/(2\delta-1)} \left(E_T \left[\frac{1}{T} \sum_{t=1}^T (y_{t+h} - \hat{\beta}'_{-h} \mathbf{w}_t)^2 \right] \right)^{(\delta-1)/(2\delta-1)} \\ &\leq CC_\delta \Lambda_{\min}^{(-\delta+1)/(2\delta-1)} \left(E_T \left[\frac{1}{T} \sum_{t=1}^T (y_{t+h} - \hat{\lambda}'_h \mathbf{w}_t)^2 \right] \right)^{(\delta-1)/(2\delta-1)} \end{aligned}$$

$$= O_p \left(\left(\frac{(\log p)^3}{T} \right)^{(\delta-1)/(2\delta-1)} \right),$$

where all the steps are analogous to deriving the bounds of $\|\tilde{\gamma}_h - \gamma_h\|_1$ except for the fourth inequality here, which comes from $\hat{J}_y \subset \tilde{J}$. Hence it follows that

$$\|\hat{\beta}_{-h} - \beta_h\|_1 = O_p \left(\left(\frac{(\log p)^3}{T} \right)^{(\delta-1)/(2\delta-1)} \right).$$

v) Bounds for $\|\tilde{\alpha}_h\|_1$

Similarly to the previous bound,

$$\begin{aligned} \|\tilde{\alpha}_h\|_1 &\leq \sqrt{\tilde{J}} \|\tilde{\alpha}_h\| \\ &\leq \sqrt{|\tilde{J}|} \|\hat{\Sigma}^{-1}(\tilde{J})\| \left\| W_h(\tilde{J})' \mathbf{v}_h / T \right\| \\ &\leq |\tilde{J}| \|\hat{\Sigma}^{-1}(\tilde{J})\| \left\| W_h(\tilde{J})' \mathbf{v}_h / T \right\|_\infty \\ &= O_p \left(\left(\frac{(\log p)^3}{T} \right)^{(\delta-1)/(2\delta)} \right) \end{aligned}$$

Now back to A and B ,

$$A - \mathbf{v}'_h \mathbf{v}_h / T \leq |\mathbf{m}' M \mathbf{m} / T| + 2 |\mathbf{m}' M \mathbf{v}_h / T| + |\mathbf{v}'_h P \mathbf{v}_h / T|$$

and

$$B - \mathbf{v}'_h \mathbf{u}_h / \sqrt{T} \leq |\mathbf{m}' M \mathbf{g} / \sqrt{T}| + |\mathbf{m}' M \mathbf{u}_h / \sqrt{T}| + |\mathbf{v}'_h M \mathbf{g} / \sqrt{T}| + |\mathbf{v}'_h P \mathbf{u}_h / \sqrt{T}|,$$

where the second and third pieces in $B - \mathbf{v}'_h \mathbf{u}_h / \sqrt{T}$ share the same bounds and $A - \mathbf{v}'_h \mathbf{v}_h / T = o_p(1)$ if $B - \mathbf{v}'_h \mathbf{u}_h / \sqrt{T} = o_p(1)$. The pieces in $B - \mathbf{v}'_h \mathbf{u}_h / \sqrt{T}$ can be bounded by

$$\begin{aligned} |\mathbf{m}' M \mathbf{g} / \sqrt{T}| &\leq \sqrt{T} \left\| M \mathbf{m} / \sqrt{T} \right\| \left\| M \mathbf{g} / \sqrt{T} \right\| \\ &= O_p \left(\left((\log p)^3 \right)^{\frac{2\delta-1}{2\delta}} T^{\frac{1-\delta}{2\delta}} \right), \\ |\mathbf{m}' M \mathbf{u}_h / \sqrt{T}| &\leq \sqrt{T} |(\tilde{\gamma}_h - \gamma_h)' W'_h \mathbf{u}_h / T| \\ &\leq \sqrt{T} \|\tilde{\gamma}_h - \gamma_h\|_1 \left\| W'_h \mathbf{u}_h / T \right\|_\infty \end{aligned}$$

$$\begin{aligned}
&= O_p \left(\left((\log p)^3 \right)^{\frac{2\delta-1}{2\delta}} T^{\frac{1-\delta}{2\delta}} \right), \\
\left| \mathbf{v}'_h P \mathbf{u}_h / \sqrt{T} \right| &\leq \left| \tilde{\alpha}'_h W'_h \mathbf{u}_h / \sqrt{T} \right| \\
&\leq \|\tilde{\alpha}_h\|_1 \sqrt{T} \|W'_h \mathbf{u}_h / T\|_\infty \\
&= O_p \left(\left((\log p)^3 \right)^{\frac{2\delta-1}{2\delta}} T^{\frac{1-\delta}{2\delta}} \right),
\end{aligned}$$

where all the pieces become $o(1)$ if $\log p = o(T^{\frac{\delta-1}{3(2\delta-1)}})$, which is satisfied by Assumption 4 (c). Therefore we have

$$\sqrt{T}(\hat{\beta}_h - \beta_h) = (\mathbf{v}'_h \mathbf{v}_h / T)^{-1} (\mathbf{v}'_h \mathbf{u}_h / \sqrt{T}) + o_p(1).$$

The remainder of the proof continues by deriving the asymptotic distribution of

$$(\mathbf{v}'_h \mathbf{v}_h / T)^{-1} (\mathbf{v}'_h \mathbf{u}_h / \sqrt{T}) = \frac{1}{\sqrt{T}} \sum_{t=1}^T v_{h,t} u_{h,t} / \tau_h^2.$$

I proceed by applying Theorem 25.12 in Davidson (2021), showing that conditions (a) – (c) hold. First, condition (a) states that $E \left[(\sum_{t=1}^T X_t)^2 \right] = 1$, where $X_t = v_{t,h} u_t / (\tau_h^2 \sigma_h \sqrt{T})$.

$$E \left[\left(\sum_{t=1}^T X_t \right)^2 \right] = \frac{1}{\tau_h^4 \sigma_h^2} E \left[\frac{1}{T} \left(\sum_{t=1}^T v_{t,h} u_t \right)^2 \right] = \frac{1}{\tau_h^4 \sigma_h^2} \Omega_h = 1.$$

Next, consider the condition (b). By Lemma 4.3 (a) and Theorem 18.9 of Davidson (2021), $\{v_{t,h} u_t\}$ is a causal L_q -NED of size $-b$, and hence of size $-1/2$. By Assumption 1 (d), it is NED on an α -mixing array $\{Y_{Tt}\}$ of size $-b/(1/q - 1/\bar{q}) < -\bar{q}/(\bar{q} - 2)$, which is satisfied by $\bar{q} > q > 2$ in Assumption 1.

The last condition (c) is on $L_{\bar{q}}$ -boundedness. From the definition of τ_h ,

$$\begin{aligned}
\tau_h^2 &= \min_{\gamma_j} \left\{ E \left[\frac{1}{T} \sum_{t=1}^T (x_{h,t} - \gamma'_h \mathbf{w}_t)^2 \right] \right\} \\
&\leq E \left[\frac{1}{T} \sum_{t=1}^T (x_{h,t} - 0' \mathbf{w}_t)^2 \right] = \frac{1}{T} \sum_{t=1}^T E[x_{h,t}^2] = \Sigma_{h,h} \leq C,
\end{aligned}$$

where 0 denotes the 0 vector and the last inequality follows by Assumption 4 (b). Also, by

Assumption 1 (b) and Cauchy-Schwarz inequality, it follows that $v_{t,h}u_t$ is $L_{\bar{q}}$ -bounded. Consider the condition (c)

$$\sup_{T,t} \left(E \left[\left| v_{t,h}u_t / \tau_h^2 \right|^{\bar{q}} \right] \right)^{1/\bar{q}} \leq \frac{1}{\tau_h^2} \sup_{T,t} \left(E \left[|v_{t,h}u_t|^{\bar{q}} \right] \right)^{1/\bar{q}} \leq C,$$

which follows from $\tau_h^2 \leq C$ and $L_{\bar{q}}$ -boundedness of $v_{t,h}u_t$.

With conditions (a) – (c) satisfied, it holds that $1/\sqrt{T} \sum_{t=1}^T v_{t,h}u_t / (\tau_h^2 \sigma_h) \xrightarrow{d} N(0,1)$, and we can obtain the desired results by applying Slutsky's theorem. \square

A.3 Proof of Theorem 4.3

Proof. Decompose

$$\begin{aligned} \left| \hat{\sigma}_h^2 - \sigma_h^2 \right| &= \left| \frac{1}{\hat{\tau}_h^4} \hat{\Omega}_h - \frac{1}{\tau_h^4} \Omega_h \right| \\ &\leq \left| \left(\frac{1}{\hat{\tau}_h^4} - \frac{1}{\tau_h^4} \right) (\hat{\Omega}_h - \Omega_h) \right| + \left| \left(\frac{1}{\hat{\tau}_h^4} - \frac{1}{\tau_h^4} \right) \Omega_h \right| + \left| \frac{1}{\tau_h^4} (\hat{\Omega}_h - \Omega_h) \right|. \end{aligned} \quad (\text{A.8})$$

From Assumption 4 (b), $1/\tau_h^4$ is bounded by a constant. I further show the probability bounds for the other components, namely $\left| \frac{1}{\hat{\tau}_h^4} - \frac{1}{\tau_h^4} \right|$, Ω_h , and $|\hat{\Omega}_h - \Omega_h|$.

First, I establish

$$\left| \frac{1}{\hat{\tau}_h^4} - \frac{1}{\tau_h^4} \right| \xrightarrow{p} 0.$$

From the definition of $\hat{\tau}_h^2$, it can be decomposed as

$$\begin{aligned} \hat{\tau}_h^2 &= \left\| (\mathbf{x}_h - W_h \hat{\gamma}_h) / \sqrt{T} \right\|^2 \\ &= \frac{1}{T} \sum_{t=1}^T v_{t,h}^2 + \left\| W_h (\gamma_h - \hat{\gamma}_h) / \sqrt{T} \right\|^2 + 2 \left| \mathbf{v}'_h W_h (\gamma_h - \hat{\gamma}_h) / T \right|, \end{aligned}$$

and we can write

$$\left| \hat{\tau}_h^2 - \tau_h^2 \right| \leq \left| \frac{1}{T} \sum_{t=1}^T v_{t,h}^2 - \frac{1}{T} \sum_{t=1}^T E[v_{t,h}^2] \right| + \left\| W_h (\gamma_h - \hat{\gamma}_h) / \sqrt{T} \right\|^2 + 2 \left| \mathbf{v}'_h W_h (\gamma_h - \hat{\gamma}_h) / T \right|,$$

where

$$\begin{aligned} \left\| W_h (\gamma_h - \hat{\gamma}_h) / \sqrt{T} \right\|^2 &= O_p \left(\left(\frac{(\log p)^3}{T} \right)^{\frac{2\delta-1}{2\delta}} \right), \\ |\mathbf{v}'_h W_h (\gamma_h - \hat{\gamma}_h) / T| &\leq \|W'_h \mathbf{v}_h / T\|_\infty \|\gamma_h - \hat{\gamma}_h\|_1 = O_p \left(\left(\frac{(\log p)^3}{T} \right)^{\frac{2\delta-1}{2\delta}} \right) \end{aligned}$$

from equations (A.6), (A.5), and (A.7). Now applying the triplex inequality to the first component by setting $x = c_1((\log p)^3/T)^{1/2}$,

$$\begin{aligned} P \left(\left| \frac{1}{T} \sum_{t=1}^T v_{t,h}^2 - \frac{1}{T} \sum_{t=1}^T E[v_{t,h}^2] \right| < c_1 \left(\frac{(\log p)^3}{T} \right)^{\frac{1}{2}} \right) \\ \leq C \exp \left(-\frac{c_1^2}{288c_M^2} \log p \right) + Cx^{-1} \exp(-c_\kappa \log p) + Cx^{-1} \exp(-c_M(\bar{q} - 1) \log p) \end{aligned} \quad (\text{A.9})$$

can be bounded by the sequence $\eta_T \rightarrow 0$ which bounds (BD1) – (BD3), because the bounds (BD1) – (BD3) grow p^2 times faster than the above bounds. Combining all three parts, we have

$$|\hat{\tau}_h^2 - \tau_h^2| = O_p \left(\left(\frac{(\log p)^3}{T} \right)^{\frac{1}{2}} \right). \quad (\text{A.10})$$

We can write

$$\begin{aligned} \left| \frac{1}{\hat{\tau}_h^4} - \frac{1}{\tau_h^4} \right| &= \left| \frac{1}{\hat{\tau}_h^2} - \frac{1}{\tau_h^2} \right| \left| \frac{1}{\hat{\tau}_h^2} + \frac{1}{\tau_h^2} \right| \\ &= \left| \frac{\hat{\tau}_h^2 - \tau_h^2}{\tau_h^4 - \tau_h^2(\hat{\tau}_h^2 - \tau_h^2)} \right| \left| \frac{\hat{\tau}_h^2 - \tau_h^2 + 2\tau_h^2}{\tau_h^4 - \tau_h^2(\hat{\tau}_h^2 - \tau_h^2)} \right| \\ &\leq \left| \frac{|\hat{\tau}_h^2 - \tau_h^2|}{\tau_h^4 - \tau_h^2|\hat{\tau}_h^2 - \tau_h^2|} \right| \left| \frac{|\hat{\tau}_h^2 - \tau_h^2| + 2\tau_h^2}{\tau_h^4 - \tau_h^2|\hat{\tau}_h^2 - \tau_h^2|} \right| = o_p(1), \end{aligned}$$

where the last bound follows from (A.10) and Assumption 4 (b).

Second, to show $\Omega_h \leq C$, I first establish that $\max_{t \leq T} E[\psi_t \psi_{t-l}] \leq C\tilde{\xi}_l$, where $\tilde{\xi}_l \rightarrow 0$ is a sequence of size $-b$. This proof follows similar reasoning found in the proof of

Lemma B.2. (ii) of [Adamek et al. \(2023\)](#). First, by Assumption 1 (d) and Lemma 4.3 (a), both $\{u_{t,h}\}$ and $\{v_{t,h}\}$ are L_{2q} -NED of size $-b$, and hence by Theorem 18.9 in [Davidson \(2021\)](#), $\{v_{t,h}u_{t,h}\}$ is L_q -NED of size $-b$ for all $h = 1, \dots, H_{\max}$. Also, by Assumption 1 (b) and Cauchy-Schwarz inequality, $\{v_{t,h}u_{t,h}\}$ is $L_{\bar{q}}$ -bounded. Applying Theorem 18.6 of [Davidson \(2021\)](#), $\{v_{t,h}u_{t,h}\}$ is an L_q -mixingale of size $-b$.

Let $k = \lfloor \ell/2 \rfloor$, and decompose $E[\psi_t \psi_{t-\ell}]$ by Minkowski's inequality.

$$\begin{aligned} E[\psi_t \psi_{t-\ell}] &\leq \left| E\left[\psi_t \left(\psi_{t-\ell} - E_{t-\ell-k}^{t-\ell+k}[\psi_{t-\ell}]\right)\right] \right| + \left| E\left[\psi_t E_{t-\ell-k}^{t-\ell+k}[\psi_{t-\ell}]\right] \right| \\ &=: A + B. \end{aligned}$$

The first term can be bounded by Hölder inequality,

$$A \leq \left| \left(E\left[|\psi_t|^{q/(q-1)}\right] \right)^{\frac{q-1}{q}} \left(E\left[|\psi_{t-\ell} - E_{t-\ell-k}^{t-\ell+k}[\psi_{t-\ell}]|^q\right] \right)^{\frac{1}{q}} \right|,$$

where the $q/(q-1)$ -th moment of ψ_t is bounded by a constant from $L_{\bar{q}}$ -boundedness, and the latter term is bounded by

$$\left(E\left[|\psi_{t-\ell} - E_{t-\ell-k}^{t-\ell+k}[\psi_{t-\ell}]|^q\right] \right)^{\frac{1}{q}} \leq C\zeta_k,$$

where ζ_k is the sequence from the Definition 4, since $\{\psi_{t-\ell}\}$ is L_q -NED of size $-b$. It follows that $\zeta_k = O(k^{-\tilde{b}}) = O(\ell^{-\tilde{b}})$ for $\tilde{b} > b$. By LIE and Hölder's inequality it holds that

$$\begin{aligned} B &= \left| E\left[E_{t-\ell-k}^{t-\ell+k}\psi_t E_{t-\ell-k}^{t-\ell+k}\psi_{t-\ell}\right] \right| \\ &\leq \left| \left(E\left[|E_{t-\ell-k}^{t-\ell+k}\psi_t|^q\right] \right)^{\frac{1}{q}} \left(E\left[|E_{t-\ell-k}^{t-\ell+k}\psi_{t-\ell}|^{q/(q-1)}\right] \right)^{\frac{q-1}{q}} \right|, \end{aligned}$$

where again the latter term can be bounded by a constant from $L_{\bar{q}}$ -boundedness, and the first term can be bounded by

$$\left(E\left[|E_{t-\ell-k}^{t-\ell+k}\psi_t|^q\right] \right)^{\frac{1}{q}} \leq \left(E\left[|E_{-\infty}^{t-\ell+k}\psi_t|^q\right] \right)^{\frac{1}{q}} \leq C\rho_{\ell-k},$$

where the first inequality follows because conditioning is a contractionary projection in L_p spaces. The sequence $\rho_{\ell-k}$ is from the Definition 2, since $\{\psi_t\}$ is an L_q -mixingale of size

$-b$. Similarly to ζ_k , it follows that $\rho_{\ell-k} = O((\ell - k)^{-\tilde{b}}) = O(\ell^{-\tilde{b}})$. Note also that ζ_k and $\rho_{\ell-k}$ are both independent of t and hence,

$$\max_{t \leq T} E[\psi_t \psi_{t-\ell}] \leq C \zeta_\ell, \quad (\text{A.11})$$

where $\zeta_\ell = O(\ell^{-\tilde{b}})$. This implies that the covariances are absolutely summable.

Now consider

$$\begin{aligned} |\Omega_h| &= \sum_{\ell=-T+1}^{T-1} \left| \frac{1}{T} \sum_{t=\ell+1}^T E[\psi_t \psi_{t-\ell}] \right| \\ &\leq 2 \sum_{\ell=0}^{T-1} \left| \max_{t \leq T} E[\psi_t \psi_{t-\ell}] \right| \leq C, \end{aligned}$$

where the last inequality follows from the absolute summability.

Finally, I show $|\hat{\Omega}_h - \Omega_h| \rightarrow 0$. First, divide it into two terms,

$$|\hat{\Omega}_h - \Omega_h| \leq |\hat{\Omega}_h - \Omega_h^K| + |\Omega_h^K - \Omega_h|,$$

where $\Omega_h^K = \sum_{\ell=-K+1}^{K-1} \frac{1}{T} \sum_{t=\ell+1}^T E[\psi_t \psi_{t-\ell}]$. Note that by (A.11), the latter term can be bounded by

$$|\Omega_h^K - \Omega_h| \leq 2 \sum_{\ell=K}^T \left| \frac{1}{T} \sum_{t=\ell+1}^T E[\psi_t \psi_{t-\ell}] \right| \leq C \sum_{\ell=K}^T \zeta_\ell \leq C \sum_{\ell=K}^T \ell^{-\tilde{b}}, \quad (\text{A.12})$$

where it converges to 0 by the following arguments. Let $\tilde{b} = b + \epsilon = 1 + (b - 1) + \epsilon$ for $\epsilon > 0$ and let $\delta = \epsilon/2$. Since $K \leq \ell$,

$$\sum_{\ell=K}^T \ell^{-\tilde{b}} \leq K^{-b+1} \sum_{\ell=K}^T \ell^{-1-\epsilon} \leq K^{1-b-\delta} \sum_{\ell=K}^T \ell^{-1-\delta},$$

and $K^{1-b-\delta} \rightarrow 0$ with $b \geq 1$ and $\sum_{\ell=K}^T \ell^{-1-\delta} \rightarrow 0$ with $K \rightarrow \infty$ and the property of p -series.

Now consider the first term. Using a telescopic sum argument, decompose

$$|\hat{\Omega}_h - \Omega_h^K| = \left| \sum_{\ell=-K+1}^{K-1} \left(1 - \frac{\ell}{K}\right) \frac{1}{T} \sum_{t=\ell+1}^T \hat{\psi}_t \hat{\psi}_{t-\ell} - \frac{1}{T} \sum_{t=\ell+1}^T E[\psi_t \psi_{t-\ell}] \right|$$

$$\leq 2 \sum_{\ell=0}^{K-1} \left(\left| \frac{1}{T} \sum_{t=\ell+1}^T (\hat{\psi}_t \hat{\psi}_{t-\ell} - E[\psi_t \psi_{t-\ell}]) \right| + \frac{\ell}{K} \left| \frac{1}{T} \sum_{t=\ell+1}^T E[\psi_t \psi_{t-\ell}] \right| \right). \quad (\text{A.13})$$

Note that from (A.11), the latter term can be bounded by

$$\sum_{\ell=0}^{K-1} \frac{\ell}{K} \left| \frac{1}{T} \sum_{t=\ell+1}^T E[\psi_t \psi_{t-\ell}] \right| \leq \frac{C}{K} \sum_{\ell=1}^{K-1} \ell^{1-\bar{b}} \leq CK^{-\bar{b}} \sum_{\ell=1}^{K-1} \left(\frac{\ell}{K} \right)^{1-\bar{b}} \leq CK^{1-\bar{b}},$$

where the last inequality comes from $\ell < K$ and $\sum_{\ell=1}^{K-1} \ell^{-1-\epsilon} \leq C$ for $\epsilon > 0$, and hence it converges to 0 since $K^{1-\bar{b}} \rightarrow 0$ for $\bar{b} \geq 1$.

Next, we turn to the first term in (A.13). From triangle inequality we have

$$\begin{aligned} & \left| \frac{1}{T} \sum_{t=\ell+1}^T (\hat{\psi}_t \hat{\psi}_{t-\ell} - E[\psi_t \psi_{t-\ell}]) \right| \\ & \leq \left| \frac{1}{T} \sum_{t=\ell+1}^T (\hat{\psi}_t \hat{\psi}_{t-\ell} - \psi_t \psi_{t-\ell}) \right| + \left| \frac{1}{T} \sum_{t=\ell+1}^T (\psi_t \psi_{t-\ell} - E[\psi_t \psi_{t-\ell}]) \right| \\ & =: A + B. \end{aligned} \quad (\text{A.14})$$

We can further write A as

$$\begin{aligned} A & \leq \left| \frac{1}{T} \sum_{t=\ell+1}^T \underbrace{(\hat{u}_t \hat{u}_{t-\ell} - u_t u_{t-\ell})}_{A(a)} \underbrace{v_t v_{t-\ell}}_{A(b)} \right| + \left| \frac{1}{T} \sum_{t=\ell+1}^T \underbrace{(\hat{v}_t \hat{v}_{t-\ell} - v_t v_{t-\ell})}_{A(c)} \underbrace{u_t u_{t-\ell}}_{A(b')} \right| \\ & + \left| \frac{1}{T} \sum_{t=\ell+1}^T \underbrace{(\hat{u}_t \hat{u}_{t-\ell} - u_t u_{t-\ell})}_{A(a)} \underbrace{(\hat{v}_t \hat{v}_{t-\ell} - v_t v_{t-\ell})}_{A(c)} \right|, \end{aligned} \quad (\text{A.15})$$

where I omit the subscript for h for simplicity. Consider the component $A(a)$ in the first and the last term. Using the baseline model specification (2.2) and the triangle inequality, we can write

$$\begin{aligned} |\hat{u}_t \hat{u}_{t-\ell} - u_t u_{t-\ell}| & \leq 2 |(\beta_h - \hat{\beta}_h) x_t u_{t-\ell}| + 2 |(\beta_{-h} - \hat{\beta}_{-h})' \mathbf{w}_t u_{t-\ell}| + |(\beta_h - \hat{\beta}_h)^2 x_t x_{t-\ell}| \\ & + 2 |(\beta_h - \hat{\beta}_h) x_{t-\ell} \mathbf{w}_t' (\beta_{-h} - \hat{\beta}_{-h})| + |(\beta_{-h} - \hat{\beta}_{-h})' \mathbf{w}_t (\beta_{-h} - \hat{\beta}_{-h})' \mathbf{w}_{t-\ell}| \\ & =: A(a)_i + A(a)_{ii} + A(a)_{iii} + A(a)_{iv} + A(a)_v. \end{aligned}$$

Each term is then bounded by

$$\begin{aligned}
\frac{1}{T} \sum_{t=\ell+1}^T A(a)_i &\leq 2 \frac{1}{T} \sum_{t=\ell+1}^T |\beta_h - \hat{\beta}_h| \max_{t \leq T} |x_t u_{t-\ell}| = O_p \left(T^{-\frac{1}{2}} \left(\frac{(\log p)^3}{T} \right)^{\frac{1}{2}} \right), \\
\frac{1}{T} \sum_{t=\ell+1}^T A(a)_{ii} &\leq 2 |(\beta_{-h} - \hat{\beta}_{-h}) W_h' \mathbf{u}_h / T| \\
&\leq 2 \|\beta_{-h} - \hat{\beta}_{-h}\|_1 \|W_h' \mathbf{u}_h / T\|_\infty = O_p \left(\left(\frac{(\log p)^3}{T} \right)^{\frac{2\delta-1}{2\delta}} \right) \\
\frac{1}{T} \sum_{t=\ell+1}^T A(a)_{iii} &\leq |(\beta_h - \hat{\beta}_h)^2| \max_{t \leq T} |x_t x_{t-\ell}| = O_p(T^{-1+\frac{1}{\bar{q}}}) \\
\frac{1}{T} \sum_{t=\ell+1}^T A(a)_{iv} &\leq 2 |\beta_h - \hat{\beta}_h| \max_{t \leq T} |x_t| \|\mathbf{w}_t\|_\infty \|\beta_{-h} - \hat{\beta}_{-h}\|_1 = O_p \left(T^{-\frac{1}{2}+\frac{1}{\bar{q}}} \left(\frac{(\log p)^3}{T} \right)^{\frac{2\delta-1}{2\delta}} \right) \\
\frac{1}{T} \sum_{t=\ell+1}^T A(a)_v &\leq \|\mathbf{Mg} / \sqrt{T}\|^2 = O_p \left(\left(\frac{(\log p)^3}{T} \right)^{\frac{2\delta-1}{2\delta}} \right),
\end{aligned}$$

where I use the \bar{q} -th moment boundedness from Assumption 1 (b), \sqrt{T} -rate for $|\beta_h - \hat{\beta}_h|$ from Theorem 4.2, and the error bounds for $|\beta_{-h} - \hat{\beta}_{-h}|$ from Theorem 4.1. Note that $|A(b)|$ can be bounded by $T^{1/\bar{q}}$ by Assumption 1 (b) and Cauchy-Schwarz inequality. Combining with $|A(b)|$, the first term in (A.15) can be bounded at the rate of $o(1)$ if $T^{-1/2+2/\bar{q}} = o(1)$, which is satisfied by Assumption 1 (b).

Turning to $A(c)$, it can be similarly expanded by (2.4) and the triangle inequality. We can write

$$|\hat{v}_t \hat{v}_{t-\ell} - v_t v_{t-\ell}| \leq |(\gamma_h - \hat{\gamma}_h)' \mathbf{w}_t v_{t-\ell}| + |(\gamma_h - \hat{\gamma}_h)' \mathbf{w}_{t-\ell} v_t| + |(\gamma_h - \hat{\gamma}_h)' \mathbf{w}_t (\gamma_h - \hat{\gamma}_h)' \mathbf{w}_{t-\ell}|,$$

and each term is bounded By

$$\begin{aligned}
\frac{1}{T} \sum_{t=\ell+1}^T |(\gamma_h - \hat{\gamma}_h)' \mathbf{w}_t v_{t-\ell}| &\leq \|\gamma_h - \hat{\gamma}_h\|_1 \|W_h' \mathbf{v}_h / T\|_\infty = O_p \left(\left(\frac{(\log p)^3}{T} \right)^{\frac{2\delta-1}{2\delta}} \right) \\
\frac{1}{T} \sum_{t=\ell+1}^T |(\gamma_h - \hat{\gamma}_h)' \mathbf{w}_{t-\ell} v_t| &\leq \|\gamma_h - \hat{\gamma}_h\|_1 \|W_h' \mathbf{v}_h / T\|_\infty = O_p \left(\left(\frac{(\log p)^3}{T} \right)^{\frac{2\delta-1}{2\delta}} \right)
\end{aligned}$$

$$\frac{1}{T} \sum_{t=\ell+1}^T |(\gamma_h - \hat{\gamma}_h)' \mathbf{w}_t (\gamma_h - \hat{\gamma}_h)' \mathbf{w}_{t-\ell}| \leq \left\| M_{\hat{\gamma}_x} \mathbf{m} / \sqrt{T} \right\|^2 = O_p \left(\left(\frac{(\log p)^3}{T} \right)^{\frac{2\delta-1}{2\delta}} \right).$$

Combining with $|A(b')|$, which can be bounded analogously to $|A(b)|$, the second term in (A.15) can be bounded at the rate of $o(1)$ if $\log p = o(T^{1-\frac{1}{\bar{q}}\frac{2\delta}{2\delta-1}})$, which is satisfied by Assumption 1 (b) and 4 (c). The third term in (A.15) is bounded at the rate of $o(1)$ if both $A(a)$ and $A(b)$ are bounded at the rate of $o(1)$, and it trivially holds by the previous arguments. Therefore, $A = o_p(1)$.

For part B, we use the triplex inequality. By Theorem 18.11 of Davidson (2021), $\{\psi_t \psi_{t-\ell}\}$ is a $L_{\bar{q}/2}$ -bounded $L_{q/2}$ -NED, and by Theorem 18.6 of Davidson (2021), $\{\psi_t \psi_{t-\ell} - E[\psi_t \psi_{t-\ell}]\}$ is a $L_{\bar{q}/2}$ -bounded $L_{q/2}$ -mixingale. Applying Lemma 4.2 with $x = c_1((\log p)^3/T)^{1/2}$,

$$\begin{aligned} P \left(\left| \frac{1}{T} \sum_{t=\ell+1}^T (\psi_t \psi_{t-\ell} - E[\psi_t \psi_{t-\ell}]) \right| < c_1 \left(\frac{(\log p)^3}{T} \right)^{1/2} \right) \\ \leq C \exp \left(-\frac{c_1^2}{288c_M^2} \log p \right) + Cx^{-1} \exp(-c_\kappa \log p) + Cx^{-1} \exp(-c_M(\bar{q}/2 - 1) \log p), \end{aligned}$$

where all three terms are bounded by $\eta_T \rightarrow 0$ used to bound (BD1) – (BD3) since the above right hand side terms grow at a slower rate, by p^{-2} . Therefore, $B = o_p(1)$ and hence (A.14) is $o_p(1)$.

So far I've shown that (A.12) and (A.13) are $o_p(1)$, and therefore we have $|\hat{\Omega}_h - \Omega_h| = o_p(1)$. Combining with other elements in (A.8), all the three terms are bounded by $o_p(1)$ and hence we accomplish $|\hat{\sigma}_h^2 - \sigma_h^2| = o_p(1)$. \square

B Proof of Lemmas

B.1 Proof of Lemma 4.2

Proof. First, consider the dependence bound from (4.4). From Lyapunov inequality and the definition of mixingales,

$$E[E[X_t | \mathcal{F}_{t-m}] - EX_t] \leq (E[|E[X_t | \mathcal{F}_{t-m}] - EX_t|^q])^{1/q} \leq c_t \rho_m,$$

and it follows that

$$(6/\epsilon) \frac{1}{T} \sum_{t=1}^T E[E[X_t | \mathcal{F}_{t-m}] - EX_t] \leq (6/\epsilon) \frac{1}{T} \sum_{t=1}^T c_t \rho_m \leq (6\bar{c}_T/\epsilon) \rho_m.$$

Now consider the tail bound in (4.4). From Hölder inequality,

$$\begin{aligned} E[|X_t| \mathbb{1}\{|X_t| > M\}] &\leq \left(E[|X_t|^{\bar{q}}] \right)^{1/\bar{q}} \left(E[\mathbb{1}\{|X_t| > M\}] \right)^{1-1/\bar{q}} \\ &\leq \left(E[|X_t|^{\bar{q}}] \right)^{1/\bar{q}} \left(P(|X_t| > M) \right)^{1-1/\bar{q}} \\ &\leq \left(E[|X_t|^{\bar{q}}] \right)^{1/\bar{q}} \left(e^{-\bar{q}M} M_X(t) \right)^{1-1/\bar{q}} \\ &\leq C^{1/\bar{q}} C^{1-1/\bar{q}} \exp(-M(\bar{q}-1)) = C \exp(-M(\bar{q}-1)), \end{aligned}$$

where the second inequality comes from Lyapunov inequality and the third and fourth from Markov's inequality and Assumption 1 (b) – (c). It follows that

$$(15/\epsilon) \frac{1}{T} \sum_{t=1}^T E[|X_t| \mathbb{1}\{|X_t| > M\}] \leq \frac{15}{\epsilon} C \exp(-M(\bar{q}-1)),$$

and hence the desired result follows. \square

B.2 Proof of Lemma 4.3

Proof. (a) Recall that $v_{h,t}$ is the projection error from equation (2.4). Since x_t and $w_{t,j}$ are L_{2q} -NED for all $j = 1, \dots, p$, the proposed result follows from Theorem 18.8 in Davidson (2021).

(b) Recall that $\epsilon_{t,h} = \{u_{t,h}, e_{t,h}, v_{t,h}\}$. I start by showing the results for $\epsilon_{t,h} = u_{t,h}$. By Theorem 18.9 in Davidson (2021), $\{w_{t,j}u_t\}$ are causal L_q -NED of size $-b$ with NED constants \tilde{d}_t and sequence $\tilde{\zeta}_m$, where

$$\tilde{d}_t = \max\{C^{1/2\bar{q}}d_t, d_t^2\}, \quad \tilde{\zeta}_m = 2\zeta_m + \zeta_m^2, \quad (\text{B.1})$$

with d_t and ζ_m defined in Assumption 1 (d).

I will proceed by showing that $\{w_{t,j}u_t - E[w_{t,j}u_t]\}$ is a causal mixingale for all $j = 1, \dots, p$, following similar arguments in the proof of Theorem 18.6 in Davidson (2021). Though $E[w_{t,j}u_t] = 0$ by Assumption 1 (a), I maintain the mean extraction to ensure

consistency across Lemma 4.3 (b) – (c). For simplicity, write $E_s^t[\cdot] = E[\cdot | \mathcal{F}_s^t]$ where $\mathcal{F}_s^t = \sigma(\varepsilon_s, \dots, \varepsilon_t)$. Also let $k := \lfloor q/2 \rfloor$, the largest integer less or equal to $q/2$. We can start from the left hand side of equation (4.1). By Minkowski's inequality,

$$\begin{aligned} \left(E \left[|E_{-\infty}^{t-m}[w_{t,j}u_t - E[w_{t,j}u_t]]|^q \right] \right)^{1/q} &\leq \left(E \left[|E_{-\infty}^{t-m}[w_{t,j}u_t - E_{t-k}^t[w_{t,j}u_t]]|^q \right] \right)^{1/q} \\ &\quad + \left(E \left[|E_{-\infty}^{t-m}[E_{t-k}^t[w_{t,j}u_t]] - E[w_{t,j}u_t]|^q \right] \right)^{1/q} \end{aligned} \quad (\text{B.2})$$

holds for all $j = 1, \dots, p$. Consider the first term.

$$\begin{aligned} \left(E \left[|E_{-\infty}^{t-m}[w_{t,j}u_t - E_{t-k}^t[w_{t,j}u_t]]|^q \right] \right)^{1/q} &\leq \left(E \left[E_{-\infty}^{t-m} \left[|w_{t,j}u_t - E_{t-k}^t[w_{t,j}u_t]|^q \right] \right] \right)^{1/q} \\ &= \left(E \left[|w_{t,j}u_t - E_{t-k}^t[w_{t,j}u_t]|^q \right] \right)^{1/q} \\ &\leq \tilde{d}_t \tilde{\zeta}_k, \end{aligned}$$

where the first inequality is the conditional Jensen's inequality and the following equality is the law of iterated expectations (LIE). The last follows from the Definition 4's equation (4.3) and (B.1). Now consider the second term in equation (B.2). Because $E_{t-k}^t[w_{t,j}u_t] - E[w_{t,j}u_t]$ is a finite lag measurable function of $\varepsilon_{t-k}, \dots, \varepsilon_t$, it is α -mixing of the same size as $\{\varepsilon_t\}$. By the mixing inequality in Theorem 15.2 in Davidson (2021),

$$\begin{aligned} \left(E \left[|E_{-\infty}^{t-m}[E_{t-k}^t[w_{t,j}u_t]] - E[w_{t,j}u_t]|^q \right] \right)^{1/q} &\leq 6\alpha_k^{1/q-1/\bar{q}} \left(E \left[|E_{t-k}^t[w_{t,j}u_t]|^{\bar{q}} \right] \right)^{1/\bar{q}} \\ &\leq 6\alpha_k^{1/q-1/\bar{q}} \left(E \left[E_{t-k}^t[|w_{t,j}u_t|^{\bar{q}}] \right] \right)^{1/\bar{q}} \\ &\leq 6\alpha_k^{1/q-1/\bar{q}} \left(E[|w_{t,j}u_t|^{\bar{q}}] \right)^{1/\bar{q}} \\ &\leq 6\alpha_k^{1/q-1/\bar{q}} C^{1/\bar{q}}, \end{aligned}$$

where α_k is the mixing coefficient, the first inequality comes from the conditional Jensen's inequality, the second from LIE, and the last from Assumption 1 (b) and Cauchy-Schwarz inequality. Combining both bounds, equation (B.2) is bounded by

$$\begin{aligned} \left(E \left[|E_{-\infty}^{t-m}[w_{t,j}u_t - E[w_{t,j}u_t]]|^q \right] \right)^{1/q} &\leq \tilde{d}_t \tilde{\zeta}_k + 6\alpha_k^{1/q-1/\bar{q}} C^{1/\bar{q}} \\ &\leq c_t \rho_m, \end{aligned}$$

where $c_t = \max\{\tilde{d}_t, C^{1/\bar{q}}\}$ and $\rho_m = 6\alpha_k^{1/q-1/\bar{q}} + 2\tilde{\zeta}_k$. The above proof applies to all

$j = 1, \dots, p$ because, for each j , $w_{t,j}$ shares the same constant $\{d_t\}$ and ζ_m by Assumption 1 (d). Therefore, $\{w_{t,j}u_t\}$ is a causal L_q mixingale with a constant c_t and sequence ρ_m for all $j = 1, \dots, p$.

Because $u_{t,h}$ and $e_{t,h}$ share the same assumptions, the same arguments apply for $\epsilon_{t,h} = e_{t,h}$. For $\epsilon_{t,h} = v_{t,h}$, because we have the NED property by (a), the rest of the proof follows the previous arguments.

(d) Since both $w_{t,j}$ and $w_{t,k}$ are L_{2q} -NED for all $j \neq k$, the same argument in the proof of (b) applies. \square

C Further Details

C.1 Finite Lag Approximation in Impulse Response Analysis

This part elaborates on the finite lag approximation in the impulse response analysis application in Section 2. When using a finite number of lags L in LP as in (2.1), the impulse response estimand from the finite lag order model necessarily includes a bias term that diminishes as L grows. To effectively approximate the infinite lags with a finite number of lags, there should be a condition on how fast p should grow so that the bias term diminishes fast enough. I will fix the notations following [Plagborg-Møller and Wolf \(2021\)](#). Denote the impulse response parameter from LP with infinite lag as β_h^* , and the finite-lag counterpart as $\beta_h^*(L)$. Define the projection residual $\tilde{x}_t = x_t - \sum_{\ell=0}^{\infty} \gamma_\ell^* w_{t-\ell}$ and the finite lag counterpart as $\tilde{x}_t(L) = x_t - \sum_{\ell=0}^L \gamma_\ell^*(L) w_{t-\ell}$. Then the following lemma holds.

Lemma 1. Assume the data $\{w_t\}$ are covariance stationary and non-deterministic, with an everywhere nonsingular spectral density matrix and absolutely summable Wold decomposition coefficients. Then, $\beta_h^* = \frac{E[\tilde{x}_t(L)^2]}{E[\tilde{x}_t^2]} \times \beta_h^*(L) + \frac{1}{E[\tilde{x}_t^2]} \left\{ \sum_{\ell=0}^{\infty} \text{cov}(y_{t+h}, w_{t-\ell}) (\gamma_\ell^* - \gamma_\ell^*(L)) \right\}$.

Proof. By the Frisch-Waugh theorem, we can write

$$\begin{aligned} \beta_h^* &= \frac{\text{cov}(y_{t+h}, \tilde{x}_t)}{E(\tilde{x}_t)} \\ &= \frac{\text{cov}(y_{t+h}, \tilde{x}_t(L)) + (\text{cov}(y_{t+h}, \tilde{x}_t) - \text{cov}(y_{t+h}, \tilde{x}_t(L)))}{E(\tilde{x}_t)} \\ &= \beta_h^*(L) \frac{E(\tilde{x}_t(L))}{E(\tilde{x}_t)} + \frac{1}{E(\tilde{x}_t)} \left(\sum_{\ell=0}^{\infty} \text{cov}(y_{t+h}, w_{t-\ell}) (\gamma_\ell^* - \gamma_\ell^*(L)) \right). \end{aligned}$$

\square

Denote the bias term as $\phi_t(L) := \frac{1}{E[\tilde{x}_t^2]} \{ \sum_{\ell=0}^{\infty} \text{cov}(y_{t+h}, w_{t-\ell}) (\gamma_{\ell}^* - \gamma_{\ell}^*(L)) \}$. The bias term shrinks as the projection coefficient $\gamma(L)^*$ get closer to γ^* . This term can be bounded by assuming that the projection coefficients for the lags later than L decays fast enough. We have

$$\begin{aligned} \phi_t(L) &= \frac{1}{E[\tilde{x}_t^2]} \left\{ \sum_{\ell=0}^{\infty} \text{cov}(y_{t+h}, w_{t-\ell}) (\gamma_{\ell}^* - \gamma_{\ell}^*(L)) \right\} \\ &\leq \frac{1}{E[\tilde{x}_t^2]} \sup_{\ell} |\text{cov}(y_{t+h}, w_{t-\ell})| \|\gamma_{\ell}^* - \gamma_{\ell}^*(L)\|_1. \end{aligned}$$

Now assume $\sup_{\ell} |\text{cov}(y_{t+h}, w_{t-\ell})| < C$ for some constant $0 < C < \infty$. For bounding $\|\gamma_{\ell}^* - \gamma_{\ell}^*(L)\|_1$, by equation (2.14) of Ing (2020), if $n|L| \leq C(T/\log^3 p)^{1/2}$ where n is the dimension of w_t , then there is some constant $0 < C' < \infty$ such that $\|\gamma_{\ell}^* - \gamma_{\ell}^*(L)\|_1 \leq C' \sum_{\ell=L+1}^{\infty} |\gamma_{\ell}^*|$. By assuming $\sum_{\ell=L+1}^{\infty} \|\gamma_{\ell}^*\|_1 = O_p(p^{-\tilde{c}})$, where $\underline{c} < \tilde{c}$ is large enough so that $(T/(\log p)^3)^{1-1/(2\delta)} p^{-\tilde{c}} = o(1)$, the bias term can be bounded: $\phi_t(L) = o_p(1)$. Note that by Assumption 4 (c), $(T/(\log p)^3)^{1/2} p^{-\underline{c}} = o(1)$. While $(T/(\log p)^3)^{1-1/(2\delta)}$ grows faster, a small increase in \tilde{c} can still bound it to be $o(1)$, as the growth rate of p is restricted at the exponential level.

C.2 Further Definitions

First, I introduce the constants defined in Section 2. This entails the assumptions (A1) and (A2) Ing (2020) used in the proof of Theorem 4.1, written in (A.2), (A.3), and (A.1). Also denote the constant c on the right hand side bound of (A.2) and (A.3) as c_1 , and the one in (A.1) as c_2 . Further denote the constant c in Assumption 4 (a) as c_3 . These constants are assumed to be some positive constants. In equation (2.9), the parameter M_T^* is defined as

$$M_T^* = \bar{c} \left(\frac{T}{(\log p)^3} \right)^{1/2\delta}, \quad (\text{C.1})$$

with a constant \bar{c} , which is some small constant that satisfies $0 < \bar{c} < \min\{\bar{\tau}, c_3\}$. $\bar{\tau}$ is defined as

$$\begin{aligned} \bar{\tau} &= \sup \tau \\ &= \sup \left\{ \tau \left| \tau > 0, \limsup_{T \rightarrow \infty} \frac{\tau c_2}{\min_{|J| \leq \tau(T/(\log p)^3)^{1/2}} \lambda_{\min}(\Gamma(J))} \leq 1 \right. \right\}, \end{aligned}$$

where $\Gamma(J) = E[\mathbf{w}_t(J)\mathbf{w}_t(J)']$ and $\lambda_{\min}(\cdot)$ refers to the minimum eigenvalue of the matrix.

Second, in equation (2.8), the parameter C^* is defined as

$$C^* > V_0 := \frac{\bar{B}(c_1 + c_2)}{\sigma_\epsilon^2}, \quad (\text{C.2})$$

where $\sigma_\epsilon^2 = \min\{\sigma_e^2, \sigma_v^2\}$ with $\sigma_e^2 = \lim_{T \rightarrow \infty} 1/T \sum_{t=1}^T e_{t,h}^2$ and $\sigma_v^2 = \lim_{T \rightarrow \infty} 1/T \sum_{t=1}^T v_{t,h}^2$. \bar{B} is defined as

$$\bar{B} > \frac{1}{\liminf_{T \rightarrow \infty} \min_{|J| \leq M_T^*} \lambda_{\min}(\Gamma(J)) - c_2 \bar{c}},$$

where \bar{c} is the constant appeared in (C.1).

D Additional Empirical Results in Section 5.2

D.1 Further Results on Debiased LASSO

In this subsection, I present additional results on the performance of debiased LASSO in the empirical applications discussed in Section 5.2. For comparison purposes, the baseline model from the main text is also included. The patterns observed in the main text persist across these alternative specifications. Debiased LASSO consistently yields highly persistent responses, particularly for inflation and inflation wedges. The unemployment response tends to be overstated, while the unemployment wedge exhibits a persistent negative skew over extended time frames. These observations raise the concerns regarding straightforward theoretical interpretation.

For a comprehensive view, the following Figures present the full array of debiased LASSO results as well as the other methods' estimates. This expanded set of findings further corroborates the notion that debiased LASSO may not be ideally suited for this particular empirical context, likely due to the low-dimensional nature of the models and the high persistence in the data.

D.2 Further Results on Good and Bad States

In this subsection, I present additional results omitted in the main text regarding the good and bad states analysis. Table 1 shows the numerical estimates and standard errors for

the results shown in Figure 10. Figures 13 through 15 illustrate the results with different dependent variables.

For both belief wedges in Figure 13 and 15, we observe positive responses immediately after the shock, which persist for a few periods, consistent with the model predictions shown in 6. In the case of unemployment, the results across various model specifications consistently exhibit a hump-shaped pattern, reinforcing the robustness of the findings across different scenarios.

Table 1: Impulse response of inflation to a pessimism shock in good and bad states

(a) Impulse response of inflation to a pessimism shock in good states

Model	Horizons (quarters)	0	1	2	3	4	5	6
Baseline	LP	0.102 (0.176)	0.288** (0.175)	0.051 (0.180)	0.061 (0.180)	0.023 (0.182)	-0.194 (0.184)	-0.103 (0.187)
	double OGA	0.077 (0.145)	0.248* (0.169)	0.009 (0.177)	0.019 (0.154)	0.023 (0.158)	-0.184 (0.167)	-0.109 (0.177)
VAR, 4 lags	LP	0 (0)	0.223* (0.155)	0.137 (0.206)	-0.544*** (0.236)	-0.333 (0.269)	-0.416* (0.282)	-0.167 (0.287)
	double OGA	0 (0)	0.102 (0.187)	0.050 (0.265)	-0.621*** (0.142)	-0.460*** (0.177)	-0.443* (0.305)	-0.594*** (0.215)
VAR, 8 lags	LP	0 (0)	0.298* (0.198)	-0.147 (0.255)	-0.910*** (0.307)	-0.354 (0.395)	-0.187 (0.397)	0.462* (0.360)
	Double OGA	0 (0)	0.081 (0.152)	-0.058 (0.253)	-0.575*** (0.158)	-0.488*** (0.171)	-0.463* (0.344)	-0.475*** (0.238)

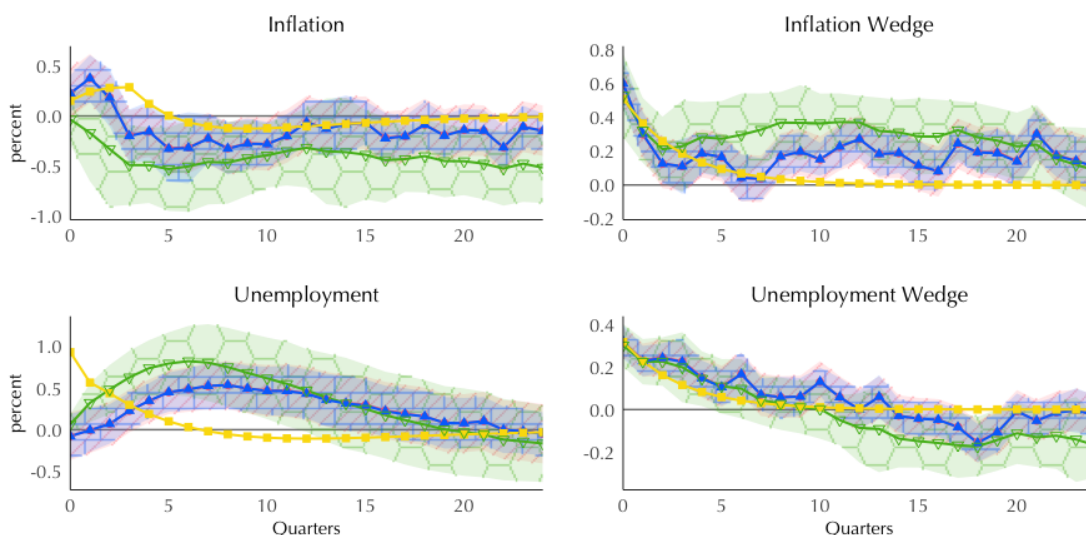
(b) Impulse response of inflation to a pessimism shock in bad states

	Horizons (quarters)	0	1	2	3	4	5	6
Baseline	LP	0.514*** (0.242)	0.579*** (0.240)	0.429** (0.246)	-0.588*** (0.245)	-0.563*** (0.246)	-0.569*** (0.249)	-0.589*** (0.253)
	double OGA	0.487*** (0.229)	0.496*** (0.146)	0.368*** (0.158)	-0.643*** (0.18)	-0.528*** (0.137)	-0.538** (0.286)	-0.555*** (0.257)
VAR, 4 lags	LP	0 (0)	0.132 (0.111)	0.051 (0.151)	0.153 (0.172)	0.173 (0.195)	-0.063 (0.205)	0.022 (0.208)
	double OGA	0 (0)	0.209*** (0.085)	0.111 (0.111)	0.046 (0.118)	0.167 (0.146)	-0.061 (0.164)	0.045 (0.174)
VAR, 8 lags	LP	0 (0)	0.196* (0.145)	0.318* (0.198)	0.191 (0.238)	0.147 (0.306)	-0.425* (0.310)	-0.788*** (0.281)
	Double OGA	0 (0)	0.156*** (0.055)	0.080 (0.107)	0.014 (0.105)	0.179* (0.139)	-0.138 (0.148)	0.013 (0.136)

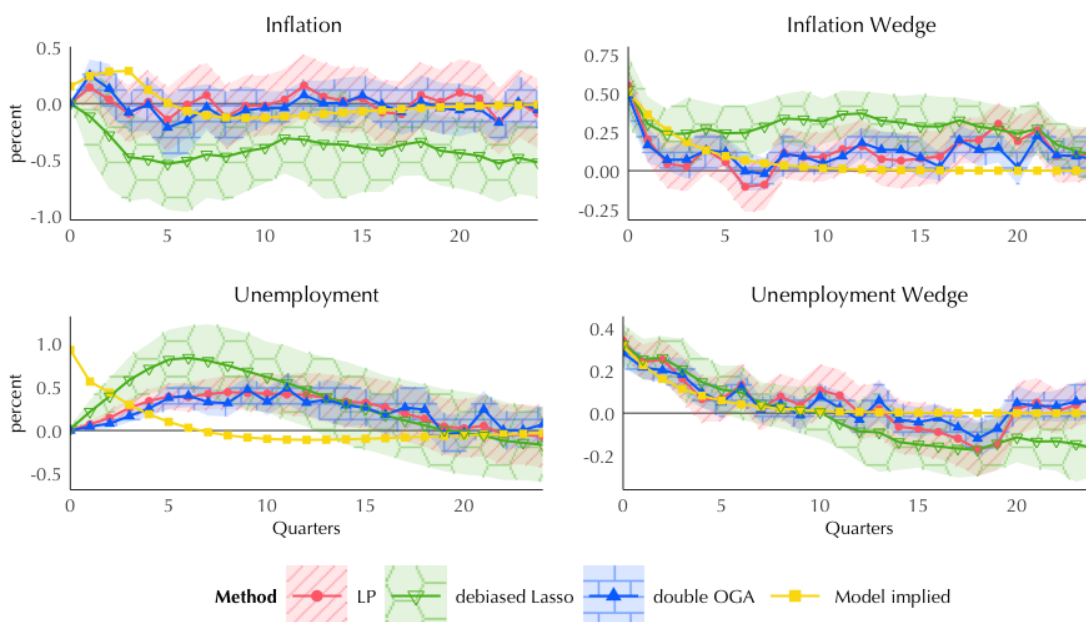
Notes. This table reports the impulse response of inflation to a pessimism shock in both good and bad states across different model specifications. Panel (a) presents the results for good states, while panel (b) shows the results for bad states. Each row corresponds to a different model: the baseline model, VAR with 4 lags, and VAR with 8 lags, using both LP and the Double OGA. The impulse responses are reported for horizons ranging from 0 to 6 quarters, with standard errors in parentheses. Statistically significant results at the 5% level are indicated by ***, 10% by **, and 15% by *.

Figure 11: Baseline and VAR controls added models with 4 lags, all methods

(a) Baseline model with 4 lags



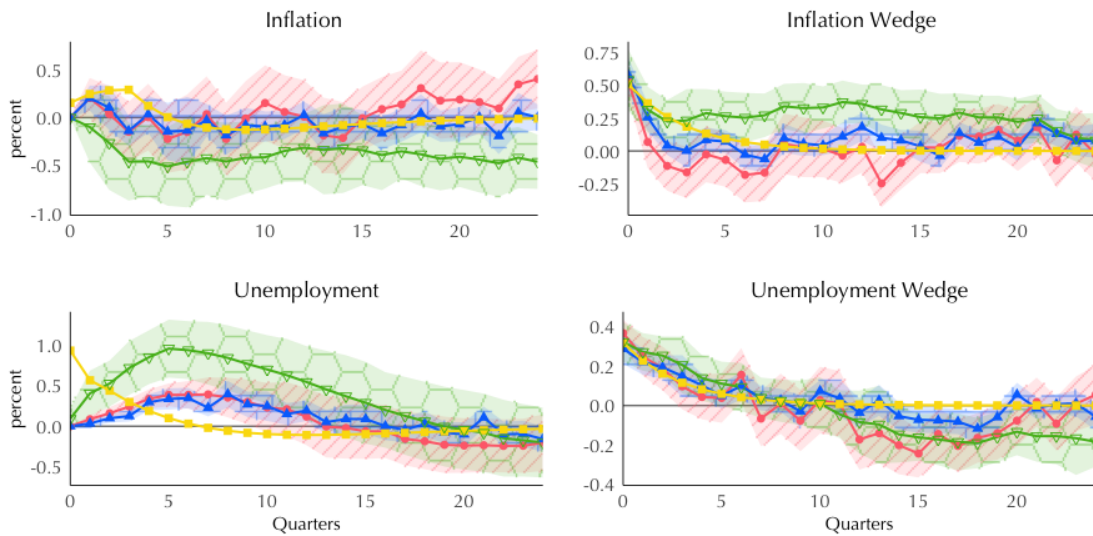
(b) VAR controls with 4 lags



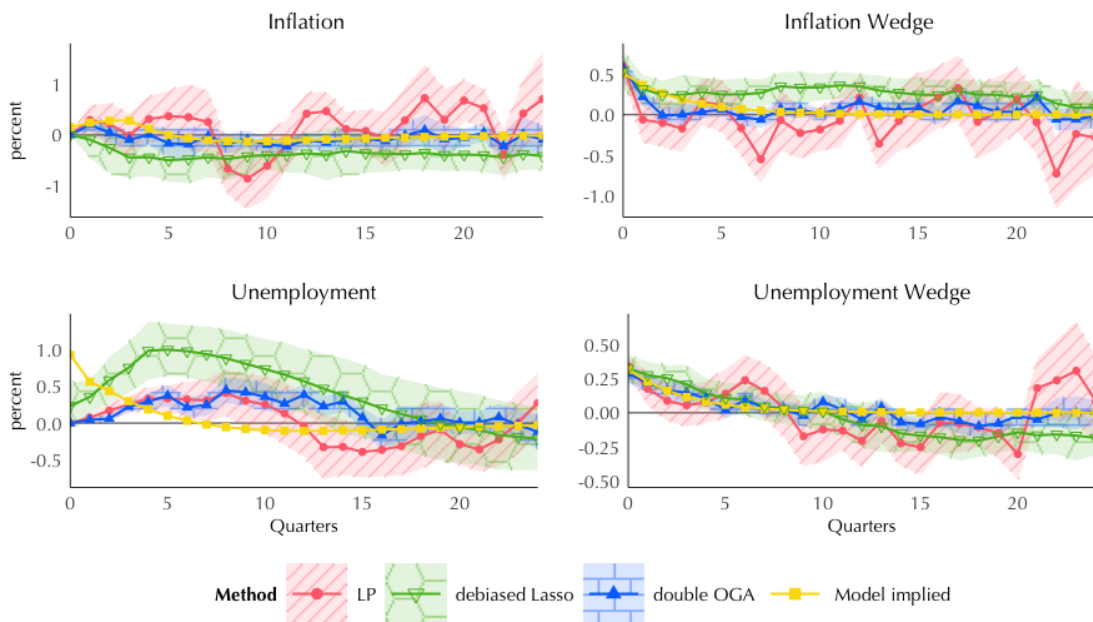
Notes. This figure compares the baseline model with 4 lags (Panel (a)) and the VAR controls added model with 4 lags (Panel (b)) for inflation, inflation wedge, unemployment, and unemployment wedge. Point estimates are shown as solid lines with circle markers for LP (red), inverted triangle markers for debiased LASSO (green), triangle markers for double OGA (blue), and square markers for model-implied (yellow). Shaded areas represent 90% confidence intervals, with diagonal shading for LP, hexagonal shading for debiased LASSO, and brick-shaped shading for double OGA.

Figure 12: VAR controls added models with longer lags, all methods

(a) VAR controls with 8 lags

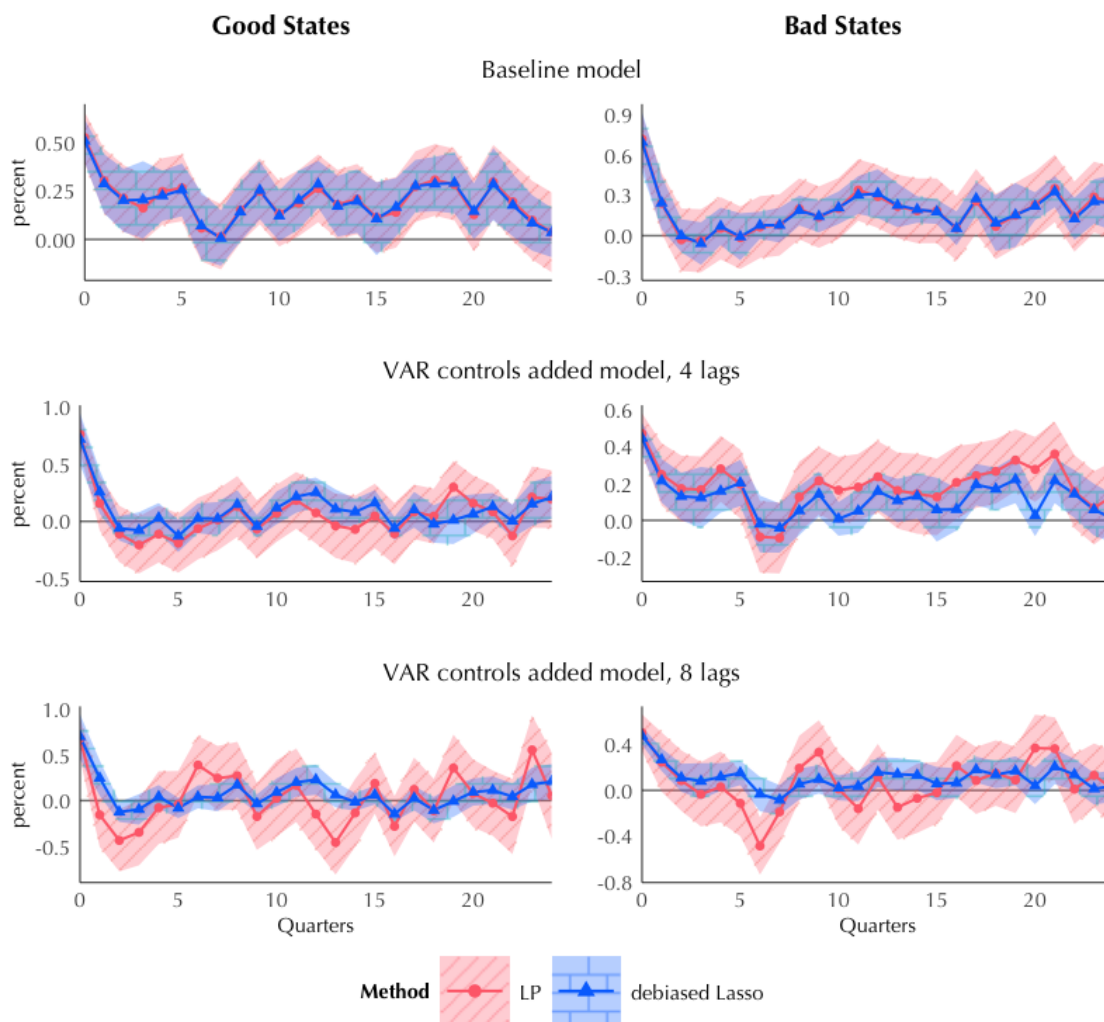


(b) VAR controls with 10 lags



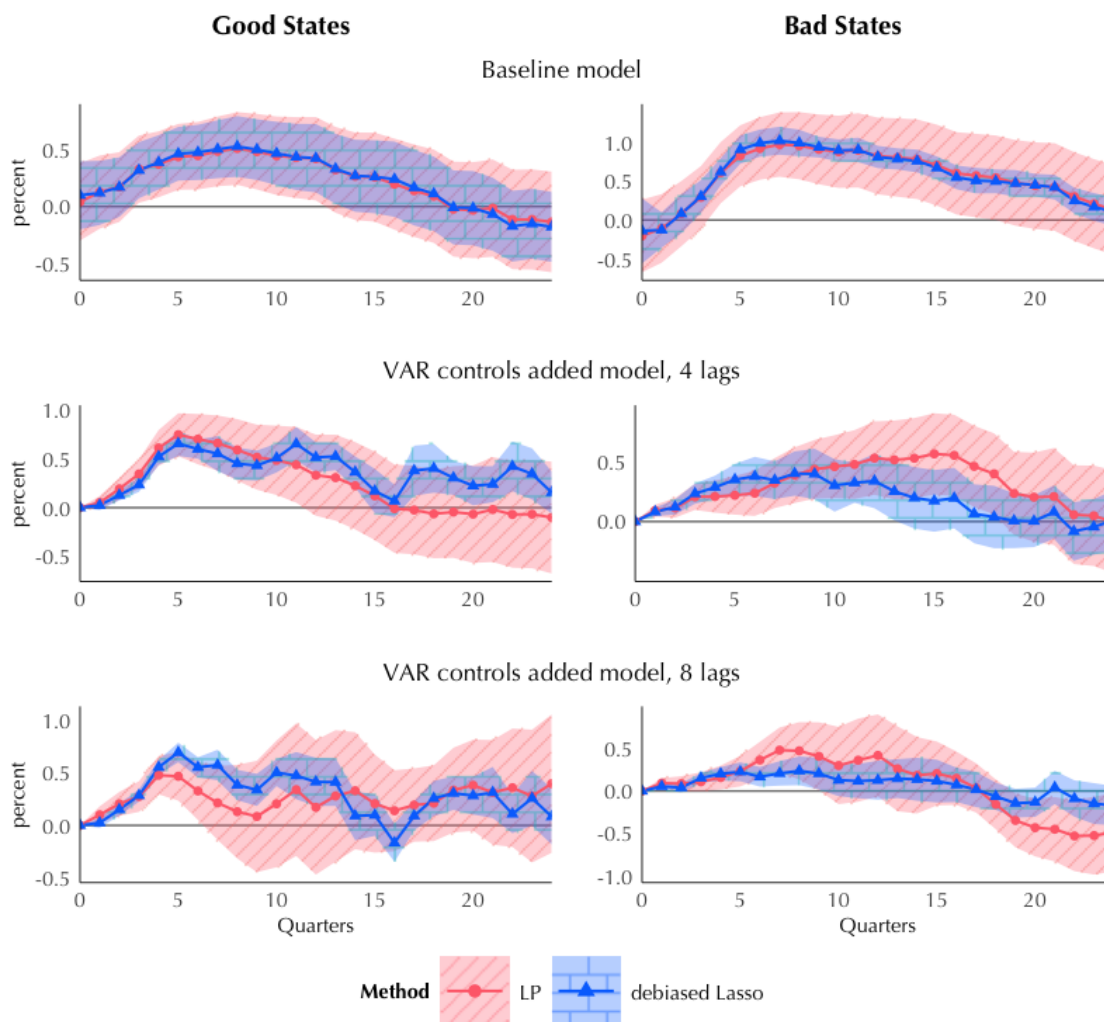
Notes. This figure compares the VAR controls added model with 8 lags (Panel (a)) and the VAR controls added model with 10 lags (Panel (b)) for inflation, inflation wedge, unemployment, and unemployment wedge. Point estimates are shown as solid lines with circle markers for LP (red), inverted triangle markers for debiased LASSO (green), triangle markers for double OGA (blue), and square markers for model-implied (yellow). Shaded areas represent 90% confidence intervals, with diagonal shading for LP, hexagonal shading for debiased LASSO, and brick-shaped shading for double OGA.

Figure 13: Impulse responses of inflation wedge with good and bad states



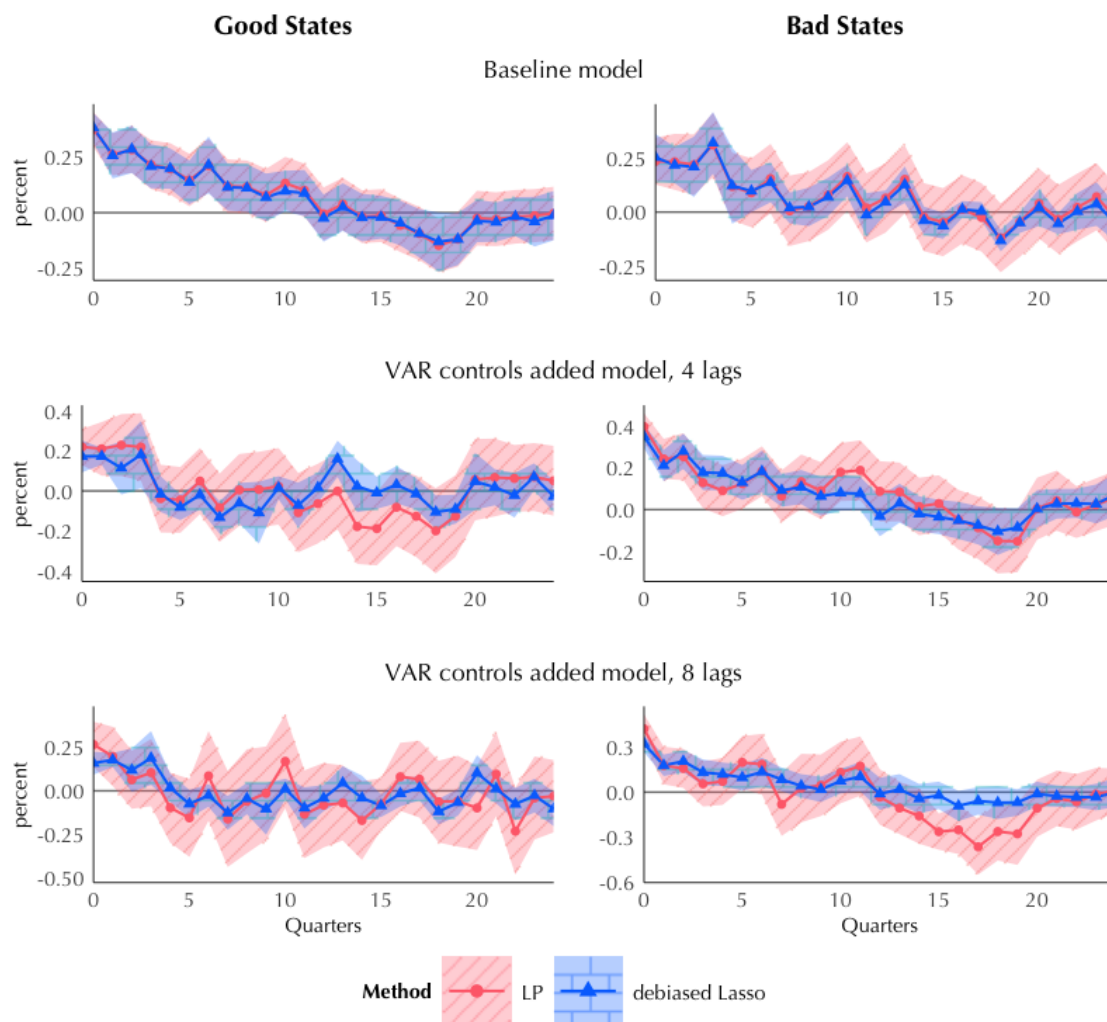
Notes. This figure illustrates the impulse responses of inflation wedge to a belief shock in both good and bad states under various model specifications. The good states (left panels) and bad states (right panels) are identified by NBER recession indicators. The model specifications include a baseline model and models with added VAR controls (4 lags and 8 lags). Point estimates are shown as solid lines with circle markers for LP (red) and triangle markers for double OGA (blue). Shaded areas represent 90% confidence intervals, with diagonal shading for LP and brick-shaped shading for double OGA.

Figure 14: Impulse responses of unemployment with good and bad states



Notes. This figure illustrates the impulse responses of unemployment to a belief shock in both good and bad states under various model specifications. The good states (left panels) and bad states (right panels) are identified by NBER recession indicators. The model specifications include a baseline model and models with added VAR controls (4 lags and 8 lags). Point estimates are shown as solid lines with circle markers for LP (red) and triangle markers for double OGA (blue). Shaded areas represent 90% confidence intervals, with diagonal shading for LP and brick-shaped shading for double OGA.

Figure 15: Impulse responses of unemployment wedge with good and bad states



Notes. This figure illustrates the impulse responses of unemployment wedge to a belief shock in both good and bad states under various model specifications. The good states (left panels) and bad states (right panels) are identified by NBER recession indicators. The model specifications include a baseline model and models with added VAR controls (4 lags and 8 lags). Point estimates are shown as solid lines with circle markers for LP (red) and triangle markers for double OGA (blue). Shaded areas represent 90% confidence intervals, with diagonal shading for LP and brick-shaped shading for double OGA.